Characterization of Coherence
in Forward-Scattered Photons in Turbid Medium
using Heterodyne Detection.

by
Changhuei Yang

Submitted to the Department of Electrical Engineering and Computer
Science

in Partial Fulfillment of the Requirements for the Degree of
Bachelor of Science in Electrical Science and Engineering
and Master of Engineering in Electrical Engineering and Computer Science.
at the Massachusetts Institute of Technology

May 19, 1997

OCT 2 9 1997

Author...
Department of Electrical Engineering and Computer
Science
May 19, 1997

Certified
by..
Michael S. Feld
Thesis Supervisor

Accepted
by..
F. R. Morgenthaler
Chairman, Department Committee on Graduate Theses

Characterization of Coherence
in Forward-Scattered Photons in Turbid Medium
using Heterodyne Detection.

by

Changhuei Yang

Submitted to the
Department of Electrical Engineering and Computer Science

May 19, 1997

In Partial Fulfillment of the Requirements for the Degree of
Bachelor of Science in Electrical Science and Engineering
and Master of Engineering in Electrical Engineering and Computer Science.

Abstract

This thesis discusses the development of a heterodyne based system designed to detect the coherent component of light transmitted through a turbid medium. The system can detect coherent light intensity as low as 100 dB of an initial sub-milliwatt level input beam. It employs a very narrow bandwidth approach for generating the required heterodyne signal so that the bandwidth of the detection is about 10 Hz, limited predominantly by vibrations of the optical components.

With this system, we studied the extent of the preservation of coherence in light that is transmitted through a turbid medium. By tilting the transmission beam by about 20 mrad, we were able to detect coherent photons which were scattered only a few times. The coherent intensity was experimentally found to be always larger than the ballistic intensity but smaller than the transmitted intensity. In addition, this coherent intensity fluctuated slowly over time. A model that assumed scattering is coherent and that the scattered light wavefront is non-uniform and fluctuating due to the Brownian motion of the microspheres, was applied and was found to be sufficient to explain the main features of the experiment.

Thesis Supervisor: Michael Feld
Title: Director, MIT G. Harrison Spectroscopy Laboratory

Acknowledgments.

Contents

List of Figures.

each photon. This experiment is done with the AOM set-up
in the signal beam arm. In this case, the sensitivity limit
is imposed by the presence of power fluctuation of the laser.

Chapter 1

Introduction.

In most previous work on scattering in turbid medium, the strategy adopted to extract imaging related information has been to profile the intensity variations of the light transmitted through the target medium. Recent experiments performed with such an approach includes time gating experiments by Alfano's group at City University of New York [1], where transmitted laser pulses are temporally resolved to isolate photons which have not undergone any scattering, also known as "ballistic" photons. Another example can be seen in Perelman's path integral approach [2], where scattered photons are profiled in time and the medium's structure is extracted by fitting the profiles obtained.

Due to the predominance of experimental work based on intensity measurements, most theoretical models are based on computing intensity profile; one of the simplifications that went into making such computation practical is that scattered light preserves no correlation to the incident light [3]. This removes the requirement on computational models to account for phase information in each possible scattering path, and allow the researchers to deal with only the intensity information of each scattering path.

In recent years, optical coherence tomography(OCT) [4][5] has been steadily developing as a practical medical approach for non-invasive imaging of biological tissues. The strategy employed here is to send a laser pulse through the biological tissue

and collect the back scattered light. By measuring the degree of coherence in the back-scattered light, we can determine the depth and characteristics of a tissue boundary within the biological sample. This approach has been demonstrated to be able to image up to a depth of 300 microns [6]. The implication of this development is that scattered light does preserve coherence to some extent.

This is in contradiction to the existing theoretical scattering models where coherence is assumed to be completely lost. It is therefore important at this point that a more detailed experimental study into the coherence of scattered light be carried out and a better theoretical model for scattering in turbid medium be developed.

The purpose of our present study is two-fold. We shall experimentally measure the extent of coherence in scattered light and, work out a qualitative theoretical model for the preservation of coherence in scattered light.

We chose to experimentally study the forward component of light scattered from few microns diameter polystyrene microspheres suspended in water, and quantify the amount of coherence or lack of in this class of scattered light. This approach has two advantages over studying back scattered light. The polystyrene microspheres are highly anisotropic scattering particles; the proportion of light forward-scattered within a very small solid angle from the incident beam is much greater than the back scattered component. This implies that the forward-scattered light will be easier to detect and its properties easier to quantify than back scattered light. In addition, by increasing the concentration of the microsphere solution, we can easily induce multipe forward-scattering in the transmitted light. Doing the same for an experiment for back-scattered light would simply complicate matters, as such increases would cause more back scatterings as well as create multiple forward-scattering on the back scattered light itself. The only major drawback with doing an experiment with forward-scattered light is that it is difficult to isolate from the incident ballistic light.

The approach we take to overcome this drawback is to detect the light transmitted at a small angle from the incident beam direction. Although the proportion of forward-scattered light is highest along the incident beam direction, a significant proportion can still be found at a small angular tilt. On the other hand, very little of the ballistic light will propagate at that direction. Therefore, tilting the detection system allows us to gather useful information about the forward-scattered light.
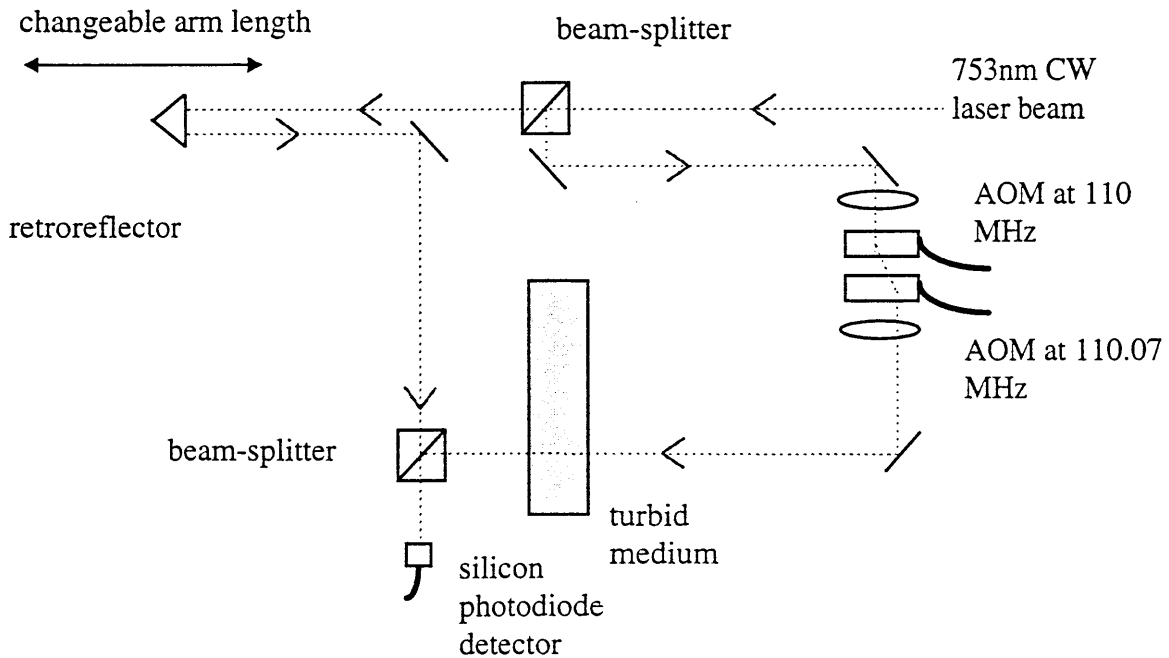
Figure 1.1: Schematic of the basic experimental set-up.

A brief outline of the experiment is presented here. The experimental set-up uses as a light source a Ti:Sapphire CW beam at 753nm. The laser beam is split into two and one beam (hereafter called the signal beam) has its frequency upshifted by 70.0 kHz through two cascaded acousto-optic modulators. The signal beam is then sent through a turbid medium of polystyrene microspheres suspended in water. The transmitted beam is recombined with the other beam (hereafter called the reference beam) from the Ti:Sapphire laser. Finally, the recombined beam is detected with a silicon photodiode and the signal is fed into a lock-in amplifier configured to pick out the 70.0 kHz signal

component. If the coherence of the transmitted laser beam is largely preserved, we should see a strong modulation in the intensity of the resulting beam at 70.0 kHz. By measuring the transmitted signal beam intensity separately, we can determine the proportion of coherent light in the signal beam. The construction of the experiment is described in detail in Chapter 2.

With this arrangement, we were able to observe the preservation of coherence in photons that have been scattered a very few number of times (about 1 - 12 times on the average). In addition, we observed that this preservation is not perfect; there exists some decoherence process which causes multiply scattered photons to have less coherence. In addition, we observed that the observed coherence fluctuates slowly over time on a time scale of 0.1 to 1 second. Chapter 3 contains a complete report of the findings from the experiments we have performed.

Our chief theoretical pursuit was to give a clear theoretical model which could account for these observations. We derived a plausible model which can explain qualitatively the observed phenomena. In the model, we attributed the observed greater loss to the more non-uniform wavefront created by the presence of scatterers. This model also explains the slow fluctuation of the observed coherence. Detailed discussion of this model is presented in Chapter 4.

In Chapter 5, we discuss in detail the experiments that we would like to conduct in the future, which should be a closer match to our theoretical model. These experiments are also expected to be easier to model theoretically, and can serve as testing grounds for the theoretical models we shall discuss in Chapter 4.

In Chapter 6, we shall summarize our findings and review briefly our objectives and outline our objectives for future experiments.

Chapter 2

Experiment Design.

The heterodyne detection of coherent light involves upshifting a component of a laser beam by a fixed frequency and then superposing the beam with an unshifted component. When the optical path lengths of the two beams are matched to within the coherence length of the laser, a modulation in the combined beam at the upshifted frequency can be seen.

This technique has two very significant advantages over simple intensity based measurement of coherent optical power; it can be used to measure very weak signals and it can isolate relevant signal from the background noise. Both advantages are extremely well suited for use in biological imaging applications [7], where the power of the optical probe beam is limited by the biological tissue tolerance and where a lot of unwanted scattering in the signal leads to large background noise.

The heterodyne technique is not limited by how small the optical power of the light beam to be measured is. By superposing with a strong enough reference beam, the weak signal beam can be magnified into regimes where it becomes measurable. Moreover, because the interaction of the two beams leads to a modulation signal which is proportional to the electric field amplitude of the signal beam, we gain by a square root factor over conventional intensity-based measurement.

The ability of the heterodyne technique to select only the component of the signal beam which has coherence with the reference beam is based on the fact that uncorrelated light sources have no common phase relationship. As such, they wash out any possible modulation pattern within a small enough time scale that it is effectively undetectable by existing photodetectors. This confers a big advantage to heterodyne detection of a small coherent signal in a large background. In conventional intensity-based measurements, there is no means for the effective isolation of the signal from the background noise.

We shall explain in detail the heterodyne set-up we built in this chapter. At the same time, we shall point out the specifications of the system and quantify the noise sources in the experiment.

2.1 Experiment Outline

The experimental set-up (see Fig. 2.1) uses a Coherent MIRA 600 Ti:Sapphire laser operating in the CW beam at 753nm as a laser source. It puts out about 1.6W of power with horizontal polarization. The beam is then directed through a pair of cross polarization beamsplitter cubes; by rotating the two with respect to each other and the polarization of the laser, we can vary the intensity of the output beam. The laser beam is then split into two at the first beamsplitter.

One of the beams (hereafter called the reference beam) propagates to a retro-reflector, and the return beam is directed via a mirror to the recombining beamsplitter. The retro-reflector is mounted on a motor-actuated translation stage capable of setting the retroreflector position with 100 micron precision. This adjustability allows us to exactly match the path length taken by the two beams. When well matched, the heterodyne signal from the recombination of the two beams will be optimal. As the coherence

14
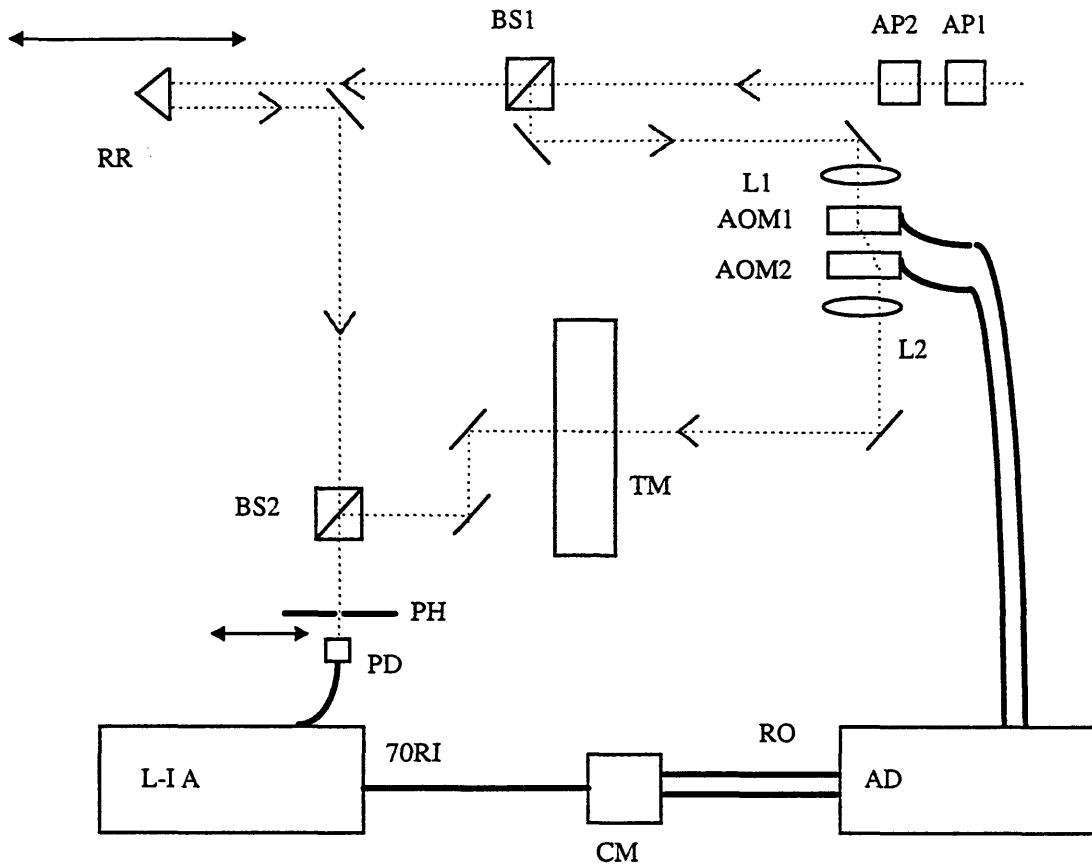
AP1,2: cross polarization beamsplitters (for attenuation)
BS1,2: beamsplitters
L1,2: convex lense (for focusing the laser in the AOMs and reshaping the beam thereafter)
AOM1,2: ISOMET 1206-C acousto-optics modulators.
RR: retroreflector
PH: width adjustable aperture
AD: IntraAction DFE-1102A4 dual frequency AOM driver
CM: VARI-L CM1 double balanced mixer
L-I A: Standford Research SR830 dual phase lock-in amplifier
PD: EG&G FND-100 silicon photodiode
RO: reference output from DFE-1102A4
70RI: reference input at 70 kHz extracted by CM-1
TM: turbid medium

Figure 2.1: Schematic of the experiment design.

length of the Ti:Sapphire is relatively long when operating in the CW mode (about 30-50 cm), finding the point where the heterodyne signal is maximum is difficult. Accordingly, we switch the Ti:Sapphire laser into mode-locking to generate picoseconds pulses. In this situation, the coherence length is short (about 0.4 mm). This allows us to match optical paths easily.

The other beam (hereafter called the signal beam) passes through a pair of ISOMET 1206C acousto-optics modulators (AOMs). The first AOM produces a +1 order Bragg diffraction beam which has a frequency upshift of about 110 MHz. The conversion of the incident beam to this frequency upshifted beam is about 60%. The 0th order beam is blocked and only the +1 order is permitted to pass to the second AOM. The second AOM is adjusted to convert about 60% of the input into a frequency downshifted -1 order. As before, the 0th order is blocked and only the -1 order is used in the rest of the experiment. The second AOM is operated at 110.07 MHz; this creates a net frequency shift of 70 kHz.

The two AOMs are driven by a custom made IntraAction DFE-1102A4 Dual Frequency Source. Because this AOM driver derives its clock frequency from a single temperature-stabilized crystal oscillator, the difference frequency from the two AOMs is much more stable than if two separate crystal oscillators were used. The manufacturer's specification in frequency fluctuations is 1 part per million. This translates to a bandwidth of about 70 mHz for the 70.0 kHz difference frequency. In the experiment, this frequency jitter is negligible compared to the frequency jitter induced by small vibrations of the optical mounts.

In addition to the two RF outputs, the driver also provide a pair of +10 dBm reference outputs. We feed these two signals into a VARI-L CM-1 double balanced mixer and extract a 70 kHz electrical signal which is exactly in phase at all times with the upshift in frequency in the laser beam. This signal is then fed to the reference input of a

Stanford Research SR830 lock-in amplifier. The detailed explanation of the function of this lock-in amplifier in our experiment shall be given later in this chapter.

The frequency upshifted signal beam is then transmitted through a turbid medium comprised of Polysciences polystyrene microspheres suspends in water. The diameters of the microspheres used in our experiment were 1.0, 4.5, 10.0 and 20.0 microns. The microspheres are manufactured with good uniformity. For example, the 4.5 microns microspheres have a mean diameter of 4.329 microns and a standard deviation of 0.269 microns. Size uniformity is required in order to ensure accurate determination of their scattering cross section and their average cosine of the deflection angle, g, through computational application of the Mie theory [8]. Given that the refractive index of water is 1.33 and the refractive index of the microspheres is 1.59, Mie theory computes a scattering cross section of 3.36×10^{-7} cm^2 and g of 0.89 for 10 micron diameter microspheres. For all diameters, the microspheres give very similar g factors. These values range from g = 0.87 for the 4.5 micron diameter microspheres to g = 0.91 for the 20 micron diameter microspheres.

Knowing the scattering cross section σ_s, the length of the beam path through the medium x, and the number density of the microspheres in the solution, n, we can easily work out the average number of scatters each photon experience as:

$$\overline{Z}_s = n\sigma_s x \qquad (2.1)$$

The attenuation of ballistic photons as they traverse the medium is given simply by:

$$I_{ballistic} / I_{ballisitc}(0) = e^{-\overline{Z}_s} \qquad (2.2)$$

This pair of equation is very important for our experiment; by steadily changing the concentration of the microsphere solution, we should be able to vary $\overline{Z}_s$. If we then plot

the normalized ballistic component of the intensity against $\overline{Z}_s$ on a log plot, we should see a linear curve. In addition, the size of the microspheres only alters the scattering cross section. Equation (2.2) is not directly dependent on the microsphere diameters; as long as we compute $\overline{Z}_s$ for each experiment, the predicted attentuation of the ballistic intensity can be found with (2.2) without further knowledge of microsphere size.

2.2 Heterodyne Detection

2.2.1 System Alignment

Two additional mirrors after the turbid medium permit us to control the direction of the beam to the recombining beamsplitter. At the beamsplitter, the reference beam and the transmitted signal beam are aligned via the mirrors to be superposed on each other. During the alignment stage of the experiment, we adjust the frequencies of the AOMs driver to confer no net frequency upshift to the signal beam. In this situation, a bulls eye interference pattern can be easily seen when the two beam are exactly parallel to and superposed on each other. (See Fig. 2.2)

This interference pattern is created by a slight divergence difference in the two beams; the divergence causes the phase difference in the beam at the center and at the first edge of the bulls eye to be π. Experimentally, we observed that the width of the center bulls eye spot is typically about 1.5 mm, though this can be improved by adjusting the lens after the second AOM to give a more collimated beam. The issue here is that the diameters of both beams are only about 2 mm wide; this leads to difficulty in visually ascertaining if the bulls eye pattern has been achieved, if the bulls eye is too wide for its surrounding destructive interference ring to show up within the diameters of the beams. This observed width gives an estimate of the divergence difference of the two beams at about 0.06 degree. In comparison, we also verified the absolute divergence by measuring

the width of the reference beam at various distances from the laser and computed that at about 0.3 degree.
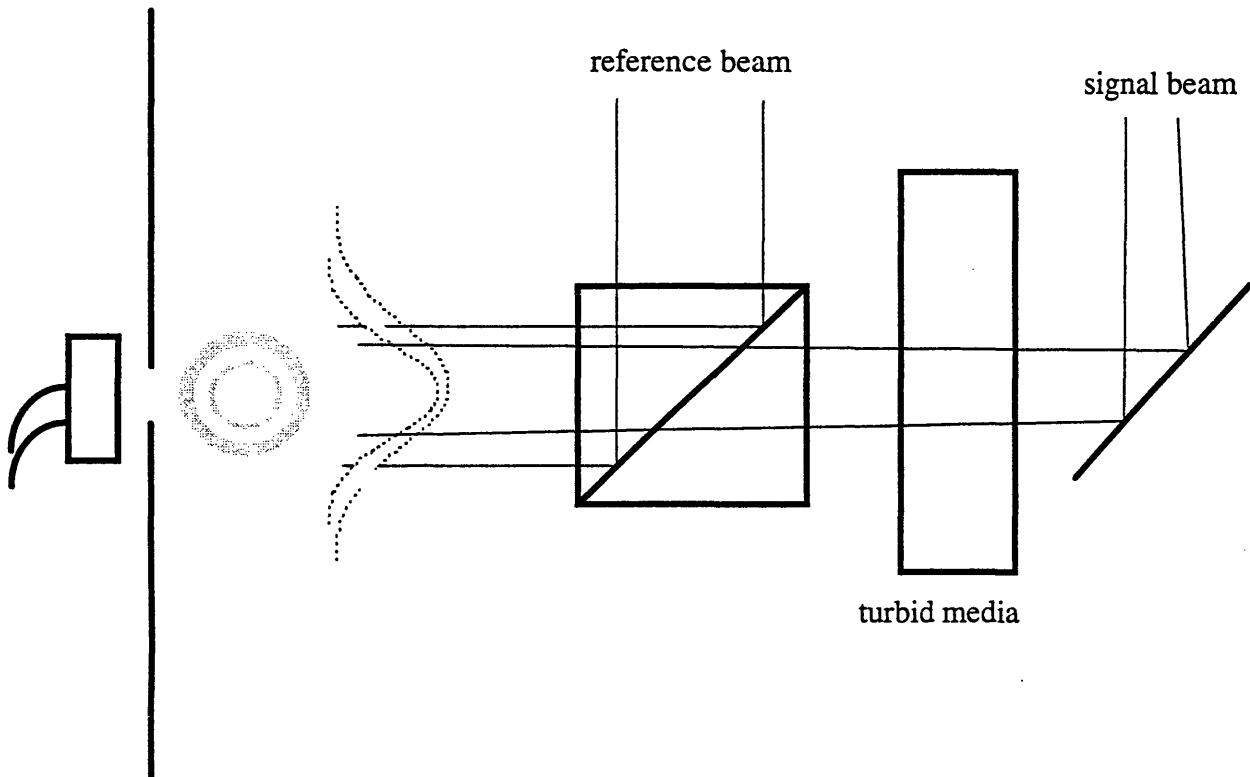
Figure 2.2: Sketch of bulls eye interference pattern with respect to the alignment of the two beams.

Having achieved a satisfactory bulls eye pattern, we then insert an adjustable aperture centered at the bulls eye. By closing the aperture to a small diameter of about 500 microns, we can effectively isolate a portion of the bulls eye such that the phase difference of the two beam at the center of the aperture is not much different from that at the edge of the aperture. This portion of the light is then received by a silicon photodiode. When the two beams are in phase with each other, the amount of light is the greatest and when they are out of phase, the portion of light received is the lowest.
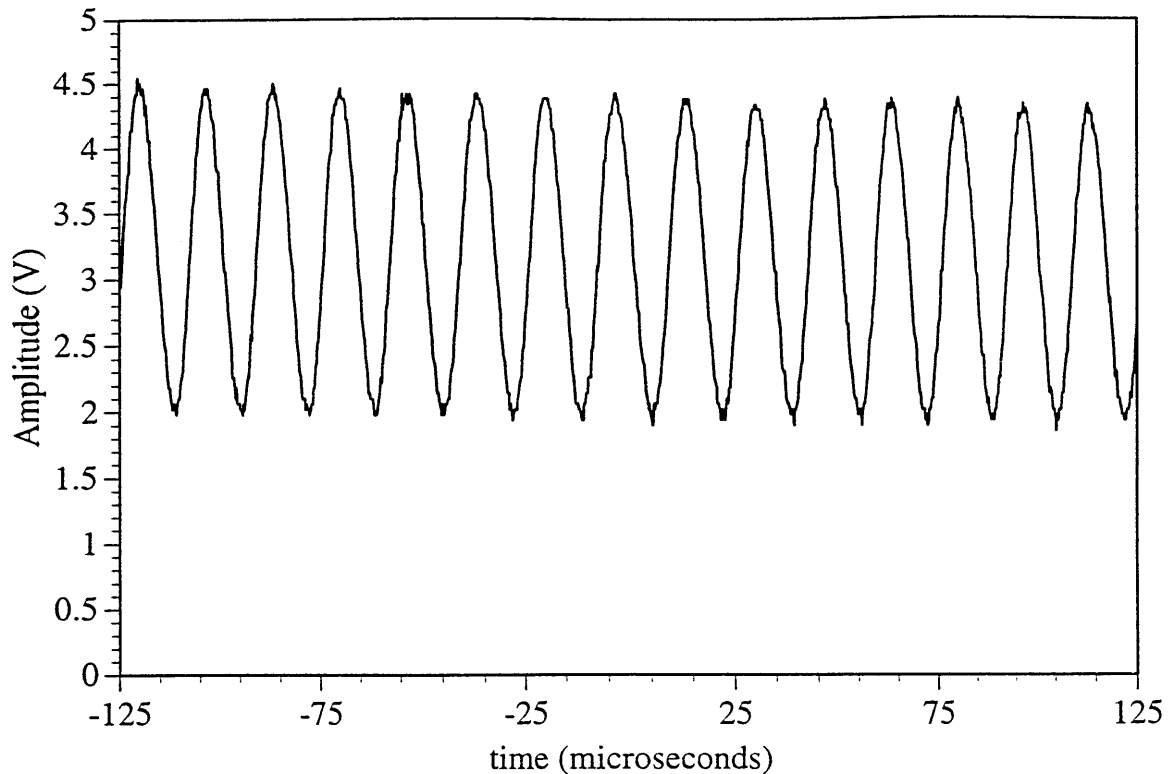
Figure 2.3: A typical heterodyne signal scan as seen on an oscilloscope.

By looking at the electrical signal on an oscilloscope, we can see that the light intensity fluctuates randomly over the time scale of seconds. This sub-Hertz fluctuation rate can be attributed to the slow thermal expansion of the various optical components, leading to translational displacements of the two beams of the order of a wavelength. In addition to this long time scale effect, there is also a visible noisy jitter at audio frequencies; there is no exact periodicity to this jitter but it is centered at roughly 200 Hz. This jitter only causes minute changes in the interference pattern intensity. It can be attributed to the sub-wavelength vibrations of the optical components in resonance with the humming from power instruments in the room such as the laser power supply. It turned out that the bandwidth of our heterodyne signal is not simply affected by the frequency of this noise source, but is also influenced by the product of the jitter frequency and the jitter amplitude. We shall return to the analysis of the contribution of this noise to

the effective bandwidth of our signal later.

2.2.2 Heterodyne Signal Computation

The AOM driver is then set so that there is a net frequency modulation of the signal beam; this causes the interference pattern to oscillate between destructive to constructive at that frequency. For the purpose of our experiment, we have chosen 70.0 kHz as the frequency upshift. Mathematically, we can write generally that

$$E_T(x,y,t) = E_r e^{i\omega t} + E_{s,coh} e^{i(\omega+\Delta\omega)t+i\theta\ (x,y,t)} + E_{s,incoh} e^{i(\omega+\Delta\omega)t+i\Gamma} \qquad (2.3)$$

where $E_T(x,y,t)$ is the electric field at the aperture, with x and y the pinhole coordinates where the electric field is calculated. In the following analysis, the light beams will be taken to be horizontally polarized, as in our experiment.

$E_r e^{i\omega t}$ represents the product of the amplitude of the reference electric field with its time-dependent phase oscillating at optical frequency, and $E_{s,coh} e^{i(\omega+\Delta\omega)t+i\theta\ (x,y,t)}$ is the same for the coherent component of the signal electric field. $\Delta\omega$ represents the frequency upshift conferred by the AOMs on the signal beam, and $\theta\ (x,y,t)$ accounts for any possible slow drifts in the relative phase of the two beams. The latter is a function of the x and y coordinates of the aperture. This is because our aperture subtends a finite area and the phase relationship at one point may be slightly different from another. $E_{s,incoh} e^{i((\omega+\Delta\omega)t+\Gamma)}$ represents possible incoherent component of the signal electric field, where Γ is a rapidly fluctuating phase leading to this field having no correlation to the either the coherent component of the signal beam or the reference beam.

The observed intensity is thus given by

$$I_T(x,y,t) = E_T^* E_T$$

$$= E_r^2 + E_{s,coh}^2 + E_{s,incoh}^2 + 2E_r E_{s,coh} \cos(\Delta\omega t + \theta(x,y,t)) \qquad (2.4)$$

$$= I_r + I_{s,coh} + I_{s,incoh} + 2\sqrt{I_r I_{s,coh}} \cos(\Delta\omega t + \theta(x,y,t))$$

where $I_T(x,y,t)$ is the intensity at the aperture averaged over a sufficiently long time so that cross terms with $E_{s,incoh} e^{i((\omega + \Delta\omega)t + \Gamma)}$ drop out as a result of Γ, but a sufficiently short time compared to the time set by $\Delta\omega$ so that we do not average out the heterodyne signal. Please note that the above equation has been normalized so that intensity can be equated to the electric field squared. Correct insertion of the electric permittivity and magnetic susceptibility is unnecessary for the treatment of this problem as the exact electric field strength amplitude is never calculated.

We then average (2.4) over the area of the aperture and derive the equation for the total collected power.

$$\bar{I}_T(t) = I_r + I_{s,coh} + I_{s,incoh} + a_P(A, \theta(x,y,t))\sqrt{I_r I_{s,coh}} \cos(\Delta\omega t + \theta'(t)) \qquad (2.5)$$

where $a_P(A, \theta(x,y,t))$ is the new scaling factor for the heterodyne signal; ideally, if the aperture is small compared to the size of the bulls eye interference pattern, then this factor will approach 2. $\theta'(t)$ is the effective phase difference.

In addition to this correction due to the finite area of the aperture, there is another correction to be made. The light is collected by an EG&G FND-100 silicon photodiode and converted to a signal current. This current is, in turn, converted to a voltage signal by placing it across a resister. Depending on the light intensity, resistor ranges from 10 kΩ to 1 MΩ with 100 kΩ being the typical value. The photodiode is rated with a capacitance of 8.5 pF, resulting in a 3 dB/octave roll-off of the system's frequency response starting at about 12kHz for a 100 kΩ resister value. This causes a reduction in the observed

22

heterodyne signal since the heterodyne signal is oscillating at 70 kHz. If we insert the reduction factor into the equation, the complete description of the observed signal becomes

$$\bar{I}_T(t) = I_r + I_{s,coh} + I_{s,incoh} + a(A,\theta(x,y,t),\Delta\omega)\sqrt{I_r I_{s,coh}} \cos(\Delta\omega t + \theta'(t)) \quad (2.6)$$

where $a(A,\theta(x,y,t),\Delta\omega)$ can be experimentally obtained. In ideal situations, $a(A,\theta(x,y,t),\Delta\omega)$ should be equal to 2.

2.2.3 Determination of Heterodyne Signal Scaling Factor

The experimental approach for determining $a(A,\theta(x,y,t),\Delta\omega)$ is as follows. First, we switch the laser into mode-locked operation. The laser pulses created in this mode are about 1.2 ps wide; their effective coherence length is calculated at about 0.4 mm. We next replace the turbid medium with water and allow the signal beam to pass unattenuated. The amplitude of the heterodyne signal is then recorded as we slowly translate the retroreflector to delay or advance the reference beam pulses with respect to the signal beam pulses. The maximum heterodyne signal is achieved when the pulses are exactly superposed temporally. By this means, we can experimentally match the arm lengths to an accuracy of about 0.1 mm, as limited by the coherence length of the laser pulses. Fig. 2.4 shows a typical scan of such an experiment.

We next switch the laser into CW mode. In this mode, the laser emits a continuous laser beam with a coherence length on the order of tens of centimeters. Still in the absence of turbid medium, the electric field component $E_{s,incoh}e^{i((\omega+\Delta\omega)t+\Gamma)}$ will be zero because there is no scattering medium that will possibly create an incoherent scattered electric field. By blocking the reference beam, we can measure the magnitude of the

signal beam intensity which, in this case, will be only $I_{s,coh}$. Likewise, by blocking the signal beam in turn, we can cmeasure I_r. The amplitude of the heterodyne signal can be measured with the use of the Stanford Research SR 830 dual phase lock-in amplifier; hereafter we shall refer to this quantity as I_{hetero}.
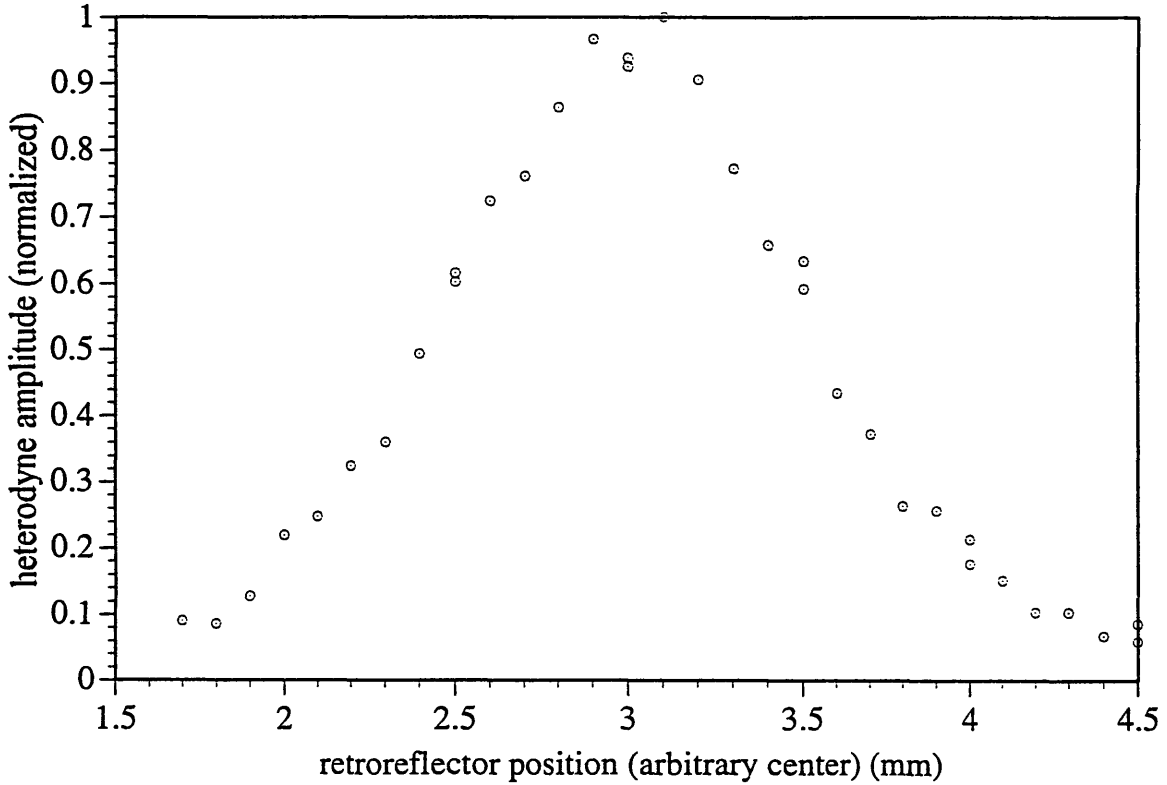
Figure 2.4: The plot of heterodyne signal amplitude versus retroreflector arm position for the laser operating in mode-locking shows a sharp position dependence which is consistent with the 0.4 mm long coherence length of the laser.

From equation 2.6, $a(A,\theta\,(x,y,t),\Delta\omega)$ can be found by the use of the three mentioned quantities by

$$a(A,\theta\,(x,y,t),\Delta\omega) = \frac{I_{hetero}}{\sqrt{I_r I_{s,coh}}}$$ (2.7)

This factor turned out in practice to have a typical value of about 0.2 for an aperture size

of 560 microns and a 100 kΩ termination resistor on the photodiode, when the two beams are well centered with respect to one another.

In order to check that this determination of $a(A,\theta\,(x,y,t),\Delta\omega)$ is accurate, we inserted a pair of cross polarization beamsplitters in the signal arm of the interferometer and used them to vary the signal beam's strength. In principle, $a(A,\theta\,(x,y,t),\Delta\omega)$ should be invariant of changes in $I_{s,coh}$. Indeed, this experiment demonstrated that $a(A,\theta\,(x,y,t),\Delta\omega)$ found this way is invariant, as shown in Fig. 2.5. The discrepancy at the end of the curve can be attributed to our inability to make accurate direct $I_{s,coh}$ measurements with the photodiode, since the intensity of the signal beam is only about 0.7 μW at that edge of the graph.
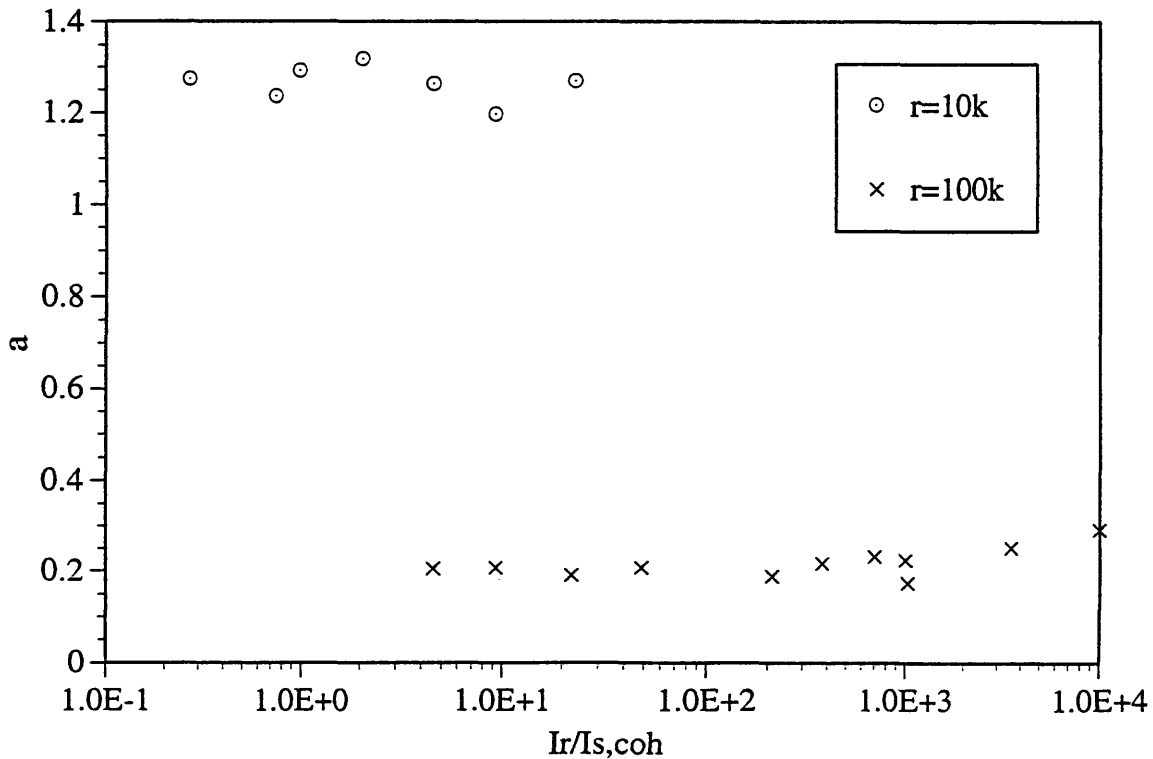
Figure 2.5: A plot of $a(A,\theta\,(x,y,t),\Delta\omega)$ for 2 different resistor values demonstrates the invariance over the ratio of $I_r/I_{s,coh}$.

Having thus determined $a(A,\theta\,(x,y,t),\Delta\omega)$, we can use equation 2.7 in the re-

expressed form of

$$I_{s,coh} = \frac{I_{hetero}^2}{a(A,\theta\,(x,y,t),\Delta\omega)^2 I_r} \qquad (2.8)$$

to determine $I_{s,coh}$ when the transmitted signal beam has a non-zero component of $I_{s,incoh}$ so that direct measurement of the intensity no longer can give $I_{s,coh}$. Hereafter, will be refered as the coherent intensity.

2.3 Bandwidth Considerations

2.3.1 Dual Phase Lock-In Amplifier

In order to address bandwidth issues of the system, we need first to understand more about the operation of the dual phase lock-in amplifier.

The Stanford Research SR 830 dual phase lock-in amplifier is a digital lock-in instrument capable of simultaneously giving the quadrature information of the signal. It operates by digitizing the input signal and multiplying the result with both a sine and cosine reference. The results are then averaged over an integration time scale as specified by the user. Finally, the two processed averages are added and its square root value displayed. This is an improvement over the single phase lock-in amplifier where the signal is processed with respect to a sine reference only. In situations where the phase of the oscillating signal drifts slowly, the dual phase amplifier will still be able to accurately give the amplitude of the oscillation while its predecessor will show a varying amplitude, becoming maximum when the signal is in phase with the sine reference and drifting to zero when the signal is in the cosine quadrature.

In effect, the dual phase lock-in amplifier acts like a Fourier transformer of the signal where the integration is performed over a time interval equal to the integration time scale. We can mathematically express the operation as

$$F_{lock-in}(\omega) = \frac{1}{T}\sqrt{(\int_0^T f(t)\cos(\omega t)dt)^2 + (\int_0^T f(t)\sin(\omega t)dt)^2}$$

(2.9)

where T is the integration time interval and f(t) is the input function.

We can find the profile of its transfer function by inserting a $2\cos((\omega + \Delta\omega)t)$ in place of f(t):

$$H_{lock-in}(\Delta\omega) = \frac{4}{T^2}\sqrt{(\int_0^T \cos((\omega + \Delta\omega)t)\cos(\omega t)dt)^2 + (\int_0^T \cos((\omega + \Delta\omega)t)\sin(\omega t)dt)^2}$$

$$= \frac{2 - 2\cos(\Delta\omega T)}{(\Delta\omega T)^2}$$

(2.10)

It can be seen that profile is roughly flat and near unity where $\Delta\omega T$ is small and drops off as $\Delta\omega T$ approaches π. More importantly, the sharpness of the transfer function is a function of the integration time interval.

The output from the lock-in can be interpreted in the frequency domain as the product of this transfer function and the frequency profile of the input signal, integrated over all frequency. It can be seen that if the input signal is sharply peaked, we can use a sharply peaked transfer function to maximize the output signal while rejecting noise over most of the spectrum. On the other hand, if the input signal is broad, a similar transfer function will not give the maximum possible output signal. The optimal solution is to select an integration time interval so that the resulting transfer function has roughly the same bandwidth as the input signal frequency profile.
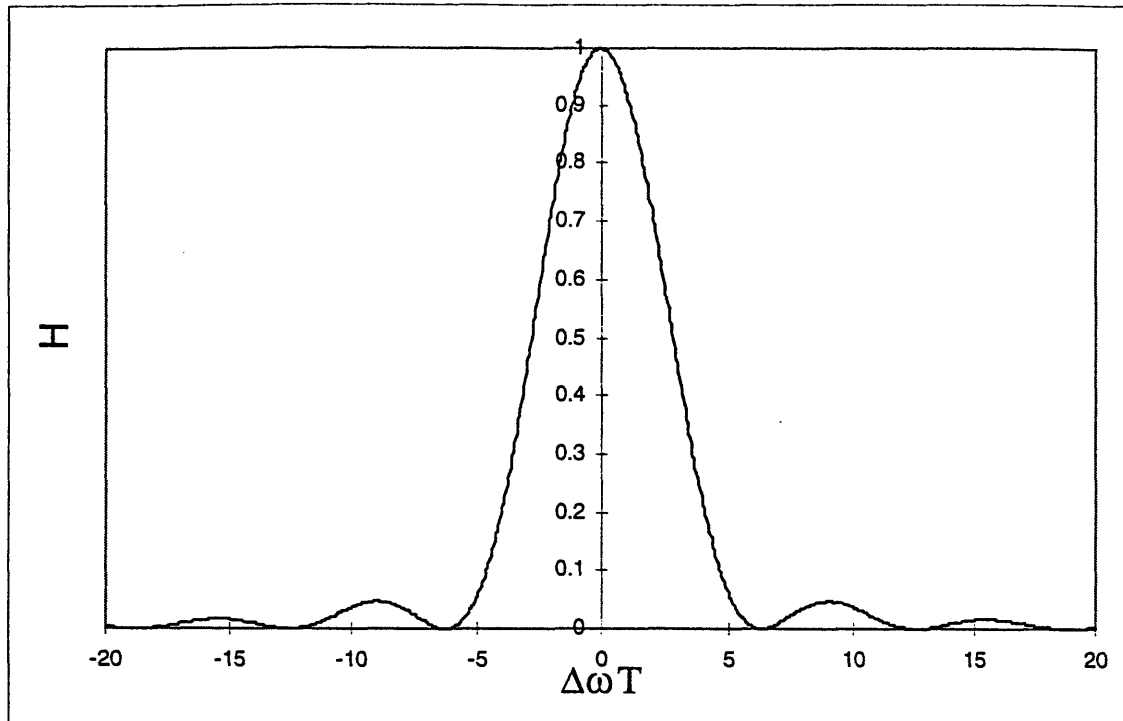
Figure 2.6: Plot of $H_{lock-in}(\Delta\omega)$ for the lock-in amplifier.

2.3.2 Frequency Jitter and Optimal Bandwidth

As mentioned earlier, the major source of broadening of the heterodyne frequency profile comes from the jitter in the optical components. A simple estimate of the broadening can be made by examining equation (2.6) with the substitution of $\theta'(t)$. At any given instant in time t, we can expand $\theta'(t + \Delta t)$ as a Taylor series projecting the evolution of $\theta'(t)$ for Δt; if we make Δt small, the first order expansion gives an adequate projection:

$$\theta'(t + \Delta t) \approx \theta'(t) + \dot{\theta}'(t)\Delta t \qquad (2.12)$$

We can substitute this into (2.6) and get

$$\bar{I}_T(t + \Delta t) = I_r + I_{s,coh} + I_{s,incoh} + a(A,\theta(x,y,t),\Delta\omega)\sqrt{I_r I_{s,coh}}\cos(\Delta\omega(t + \Delta t) + \theta'(t + \Delta t))$$

$$\approx I_r + I_{s,coh} + I_{s,incoh}$$

$$+ a(A,\theta(x,y,t),\Delta\omega)\sqrt{I_r I_{s,coh}}\cos(\Delta\omega t + \theta'(t) + (\Delta\omega + \dot{\theta}'(t))\Delta t)$$

$$(2.13)$$

We can see that $(\Delta\omega + \dot{\theta}'(t))$ can be interpreted as the instantaneous frequency of the heterodyne signal. The wider the ranging of $\dot{\theta}'(t)$ is, the broader the frequency profile of the heterodyne signal will be.

An estimation of the frequency profile broadening by slow jitter in the optical component can be made by using the experimentally observed time for the drifts of the bulls eye interference pattern from constructive to destructive. That observed time is about 1 second and the phase change is π. This gives a typical $\dot{\theta}'(t)$ of about 3.1 s^{-1}. In terms of frequency broadening, this translates to a linewidth of 0.5 Hz. In comparison, the faster jitter in the audio frequency range mentioned earlier has a phase change of about 25% of π and shows a time scale of about 5 ms. This gives a typical $\dot{\theta}'(t)$ of about 157 s^{-1}. This translates to a linewidth of 25 Hz in terms of frequency broadening.

In terms of appropriate integration time scale that would give optimal performance, we should therefore chose one with a transfer function of bandwidth comparable to 25 Hz or effective interval of about 40 ms.

We performed an experiment to verify this estimate. By removing the turbid medium, we are able to get a strong heterodyne signal from the detector. Because of its high signal level, noise does not affect measurements much. We then measure the heterodyne signal for various different integration time interval. When the bandwidth of the lock-in amplifier's transfer function is wider than the linewidth of the heterodyne signal, we should see an output that is about the size of the input heterodyne signal. As

we increase the integration time interval, the corresponding narrowing of the transfer's bandwidth eventually reaches a point where the transfer's bandwidth is narrower than the heterodyne signal. At and beyond this point, the output should show a decrease as part of useful heterodyne signal in the frequency regime is no longer accepted by the transfer function. In addition, this point of roll-off should occur at about 40 ms, as this time factor defines the linewidth of the heterodyne signal.
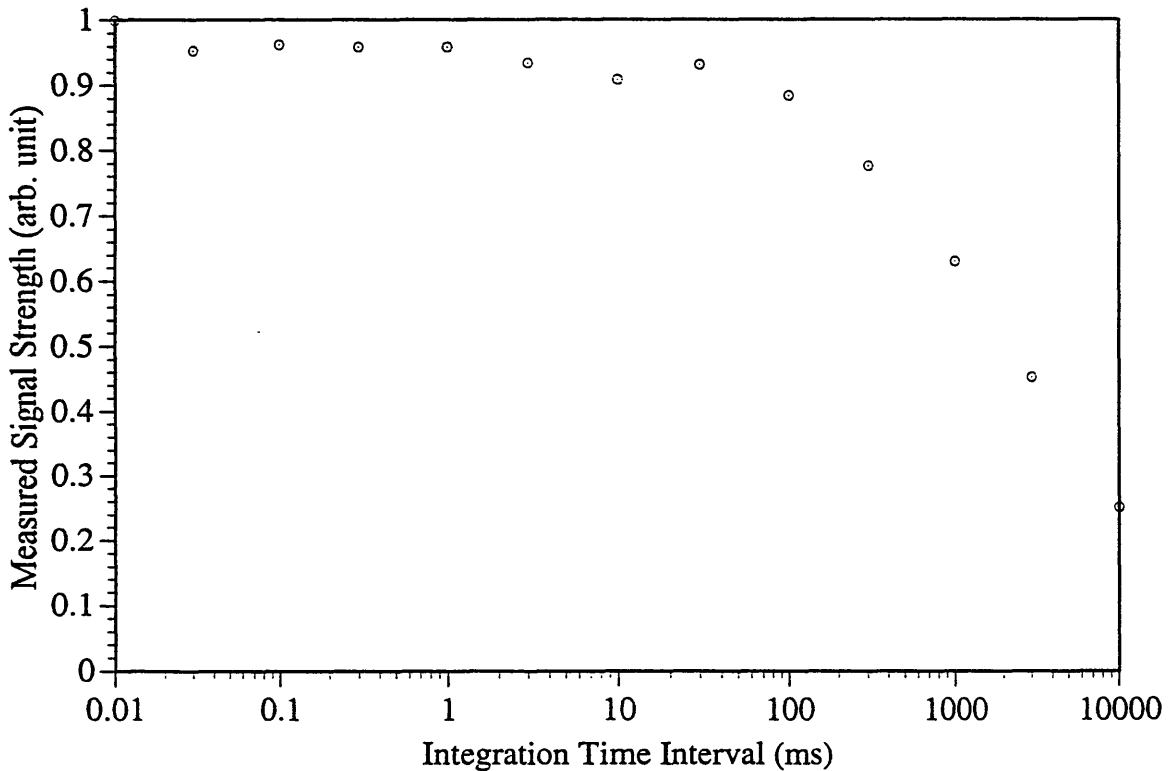
Figure 2.7: Lock-in amplifier's output shows a reduction when the integration time interval defines a bandwidth narrower than the heterodyne signal linewidth.

As can be seen in the data gathered from the experiment shown in Fig. 2.7, all the features predicted do indeed appear in the experiment. The slight discrepancy in the roll-off frequency which occur at an integration time interval of about 100 ms from our prediction of 40 ms is justifiable in the light of the fact that the prediction was made with physical quantities which are only measured with order of magnitude accuracy.

2.3.3 Comparison with Other Heterodyne Systems

The effective linewidth of about 10 Hz in the heterodyne signal represents a very significant improvement over previous heterodyne systems. For example in the original optical heterodyne microscope [9], the bandwidth achieved was about 700 kHz. In that experiment, the frequency upshift mechanism was a single AOM driven at 70 MHz. The resulting heterodyne signal at 70 MHz was bandpassed, and the resulting signal measured for its modulation envelop. In a more recent optical coherence reflectometry experiment [6], the bandwidth was narrowed to 9.1 kHz. In this case, the frequency upshift was created by rapidly varying one of the interference arms thereby inducing a rapid phase shift which behaved like a frequency upshift. Again, the heterodyne signal was bandpassed and its modulation envelop measured.

In an earlier version of our experiment, we tried to drive the AOMs with separate drivers. These drivers were ISOMET D323 110 MHz AOM drivers referenced to crystal oscillators. In the experiment, we observed a net jitter of the heterodyne signal of about 0.9 kHz. This frequency instability, though itself was an improvement over previous published experiments, was significant enough that the lock-in amplifier could not set its reference in tandem with the heterodyne signal. The problem can be attributed to the inherent frequency instabilities in the crystal oscillators. When operating at 110 MHz, the frequency instability is about 1 kHz. While this instability is only a small fraction of the center frequency at 110 MHz, it is no longer insignificant when we cascade two AOM to obtain an operating frequency of 70 kHz.

This problem was solved by the replacement of the two driver units with a custom made single driver. As mentioned earlier, the IntraAction DFE-1102A4 dual frequency source has as its reference only one crystal oscillator. The reference frequency from the crystal is processed digitally to provide the two slightly different frequencies for the two

31

AOMs driving sources. Due to this common reference, any frequency drifts is shared by both AOMs and are largely eliminated from the upshifted laser beam. This new instrument thus makes it possible for us to achieve a linewidth in the heterodyne signal which is limited by the vibrations of optical components.

This narrow linewidth allows for better signal to noise ratio in the detection of our signal.

2.4 Noise Considerations

2.4.1 Quantum Shot Noise

If the input signal is confined within a narrow frequency spectrum, the bandwidth of the lock-in as set by the integration time scale can be made narrow without losing the signal. A narrow bandwidth has the advantage that noise in the rest of the spectrum is rejected.

The fundamental limit of the signal to noise ratio is given by the quantum shot noise limit. Simply put, it is from the graininess in the measurement current due to the discreteness of the electron charge. In other words, current cannot take all possible values but rather possess discrete values as dictated by the charge of the electron.

The formulation of the quantum shot noise limit can be found in various texts. We shall presently give a brief outline, details of this formulation can be looked up in references 9 and 10. The shot noise in current fluctuation due to an average intensity I over an area of A is given by:

$$\left\langle i_{SN}^{2} \right\rangle = 2 \frac{e^{2} \eta}{\hbar \omega} \Delta f I A \qquad (2.14)$$

where e is the electron's charge, η is the quantum efficiency of the detector, $\hbar$ is Planck's constant, ω is the optical frequency and Δf is the bandwidth accepted as the signal spectrum. $\frac{e \eta}{\hbar \omega}$ constitute the ratio of conversion of optical power into the photodetector current and we can express the average current from the photodetector as

$$i_{ave} = \frac{e \eta}{\hbar \omega} I A \qquad (2.15)$$

In heterodyne signal detection, we are looking for a small modulation signal sitting upon the much bigger average intensity. This modulation signal has a RMS value in current as given by:

$$\left\langle i_{S}^{2} \right\rangle = (\frac{e \eta}{\hbar \omega})^{2} (rmIA)^{2} \qquad (2.16)$$

where r is the roll-off factor in the photodetector in response to the frequency of the heterodyne signal and m is the fractional modulation of the optical power.

The limit of the detectability of the heterodyne signal occurs when (2.14) equals (2.16) where the heterodyne signal becomes comparable to the shot noise and is given by:

$$\frac{S}{N} = \frac{\left\langle i_{S}^{2} \right\rangle}{\left\langle i_{SN}^{2} \right\rangle} = \frac{(\frac{e \eta}{\hbar \omega})^{2} (rmIA)^{2}}{2 \frac{e^{2} \eta}{\hbar \omega} \Delta f I A} = \frac{(rm)^{2} i_{ave}}{2 e \Delta f} = 1 \qquad (2.17)$$

Notice that the appearance of the bandwidth on the denominator implies that we can detect a weaker heterodyne signal if it has a narrower bandwidth. Our efforts in

narrowing the bandwidth with the use of a dual source frequency driver and the lock-in amplifier are aimed towards this narrowing of bandwidth to allow detection of weaker heterodyne signals.

In our experiment, the reference beam intensity typically defines the constant I; the signal beam is extremely weak compared to the reference beam intensity in the weak heterodyne detection situation. The typical reference power of about 0.65mW from our experiment gives a photocurrent of about 0.39 mA. The typical bandwidth of the lock-in amplifier is about 10 Hz. Putting these two values into equation (2.17), we find that the minimum detectable heterodyne signal is given by 24.9 pA. In reality, we see a noise level of about 1400 pA. Equivalently, we are seeing a noise level which is about 60 times higher than the quantum shot noise limit. In terms of coherence intensity detectability, these numbers implies that the minimum coherent intensity detectable is about 130 dB below the initial input intensity.

It is very likely that this noise is due largely to power fluctuations in the laser. At present, we have no stabilization systems to compensate for this noise. We are looking into setting up a dual balanced detection system to cut down this noise. In the dual balanced detection system, we can do active noise cancellation by subtracting any power fluctuations from the input signal by detecting the power of the laser via another photodetector. Any fluctuations that arises from the laser itself will appear at both photodetectors and can be canceled out while the heterodyne signal will be manifested only in the main experimental set-up.

2.4.2 Acousto Optic Modulators Mixed Noise

It turns out that there is a more serious noise problem in our system: the AOM mixed noise. In essence, this problem arises because the 0th order beam emerging from

an AOM blends to some extent into the ±1 order beams.

This creates a situation where a portion of the light in the 0th order beam from the first AOM gets into the second AOM along with the +1 order beam. Part of this light is again transmitted in the 0th order and it blends into the -1 order beam again. The net result is that we have a strong laser beam with a net upshift of 70 kHz from the +1 order to -1 order transmission and a much weaker superposed beam from 0th order to 0th order transmission.

Overlap of the 0th order beam with the +1 order.

Overlap of the 0th order beam with the -1 order.
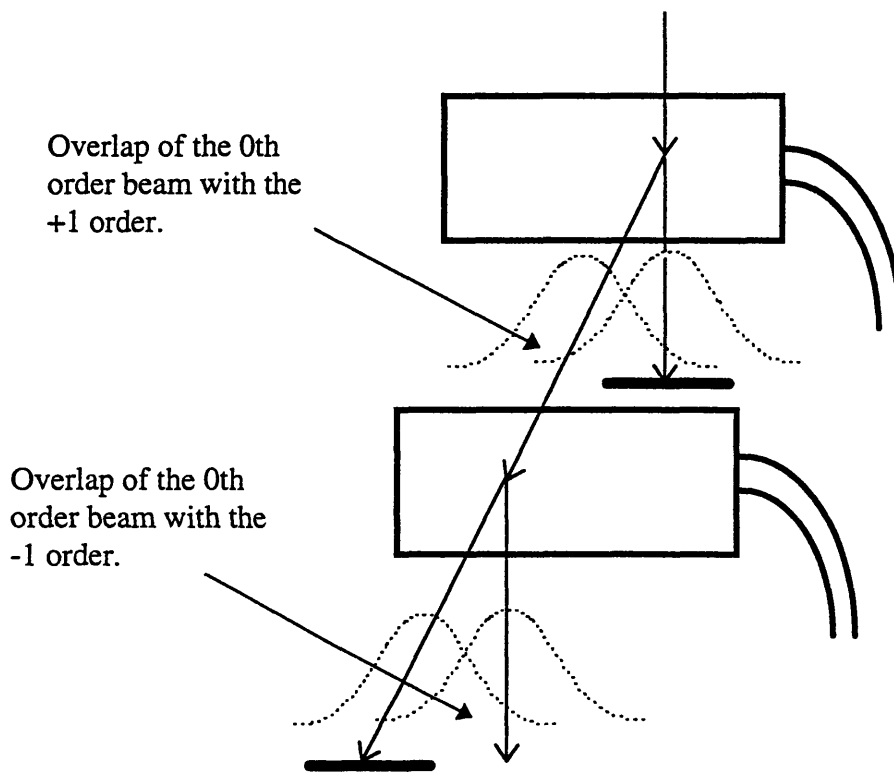
Figure 2.8: An illustration of the blending problem in the AOM set-up.

When we detect the signal from the transmission from the AOM set-up, the two superposed beams give a weak heterodyne signal at 70 kHz. There are two hallmarks of this blending induced heterodyne signal. First, there is no need to impose a reference

beam on this signal beam to get the heterodyne signal; it is manifested even when we have only one beam. Second, there is no phase drift in this heterodyne signal in time. The phase drifts in the original heterodyne signal are induced by movements of the optical components; in this case, the two superposed beams interact with the same set of optical components. Thus, they experience the same amount of phase drifts together and have no differential phase difference between them.

This blending effect can be minimized by optimizing the conversion of the incident beam into the ± 1 order beams, thereby reducing the amount of optical power in the 0th beam. With our best efforts, we are able to get to the point where a mean photocurrent of about 98 μA gives a heterodyne signal of amplitude equals to 0.11 μA with a 10 $k\Omega$ termination resister on the photodiode. We can estimate the strength of the blended 0th order to 0th order transmission by using the following equation derived from heterodyne equation (2.8). In this case, $a(A, \theta\ (x, y, t), \Delta\omega)$ can be replaced by 2, as there is little frequency roll-off in the heterodyne signal with the low valued termination resistor and the two beams can be well approximated as being exactly parallel to each other. This gives a ratio of 1.3×10^{-6} for the power of the undesired 0th order to 0th order transmission to the +1 order to -1 order transmission.

This can represent a significant problem in our experiment. If we use the AOM arrangement on the reference arm, a situation can arise in which the weak coherent signal transmitted through the turbid medium becomes comparable in power to this +1 order to -1 order transmission. In this case, our heterodyne signal will be significantly distorted by this unwanted heterodyne from this +1 order to -1 order transmission.

As such, we placed the AOM set-up at the signal arm. This way, scattering reduction of the signal beam as it passes through the medium also reduces the unwanted 0th order to 0th order transmission correspondingly. By this means, we are able to get around this problem.
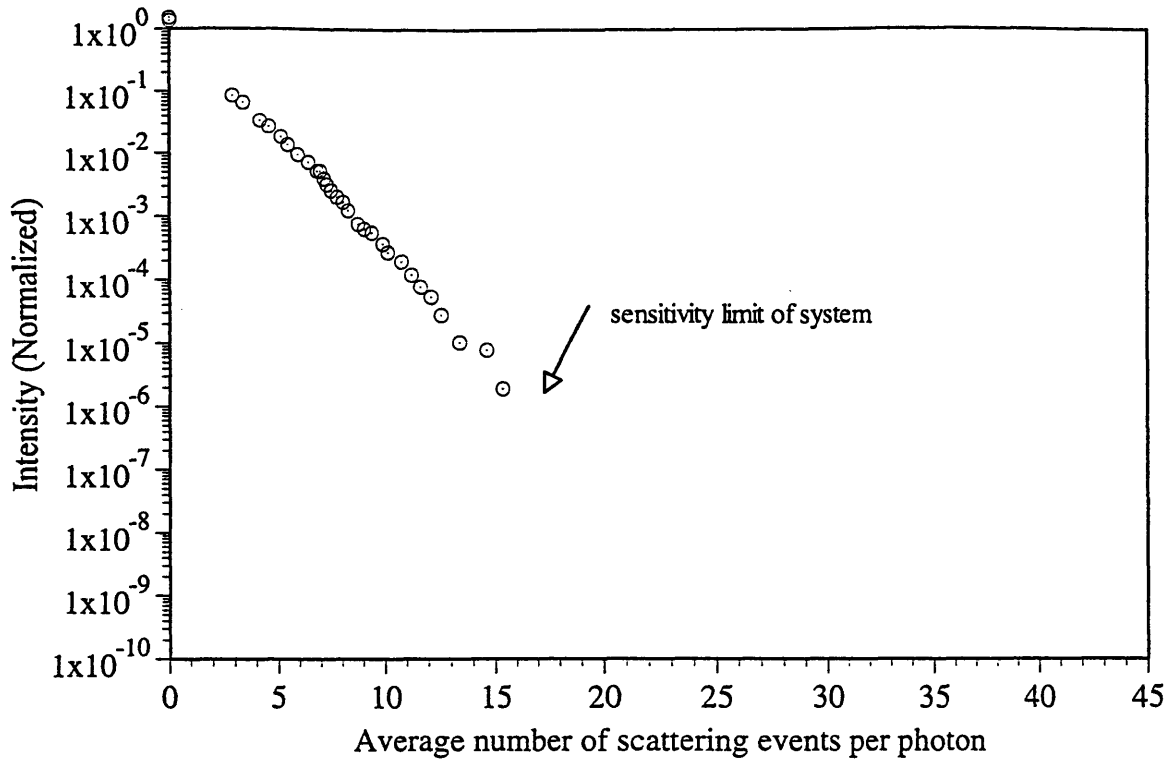
Figure 2.9: Plot of the normalized coherent light intensity versus the average number of scattering events within the turbid medium for each photon. This experiment is done with the AOM set-up in the reference beam arm. The sensitivity limit is imposed by the presence of unwanted 0th order to 0th order transmission.

A demonstration of the improvement to our ability to detect the coherent component of the transmitted light using such an arrangement can be seen in Fig. 2.9 and 2.10. In each experiment, the concentration of the turbid medium is increased. The transmitted coherent light is attenuated correspondingly. Our ability to detect smaller coherent power increased by about 40 dB as a result of the switch of the AOM set-up to the signal arm.

A more permanent fix of the problem is to eliminate the blending of the 0th order beam into the ±1 order beams. Such can be achieved by allowing the beams exiting from each AOM to travel a longer distance thereby separating the beams out further before we block off the unwanted beams. Unfortunately, the space on the experiment table is limited

and we need a bigger space before such can be attempted. Another possible solution would be to increase the power to the AOMs. By doing such, the conversion of the input beam into the ±1 order beams will be more complete; this will correspondingly reduce the intensity of the 0th order beam.
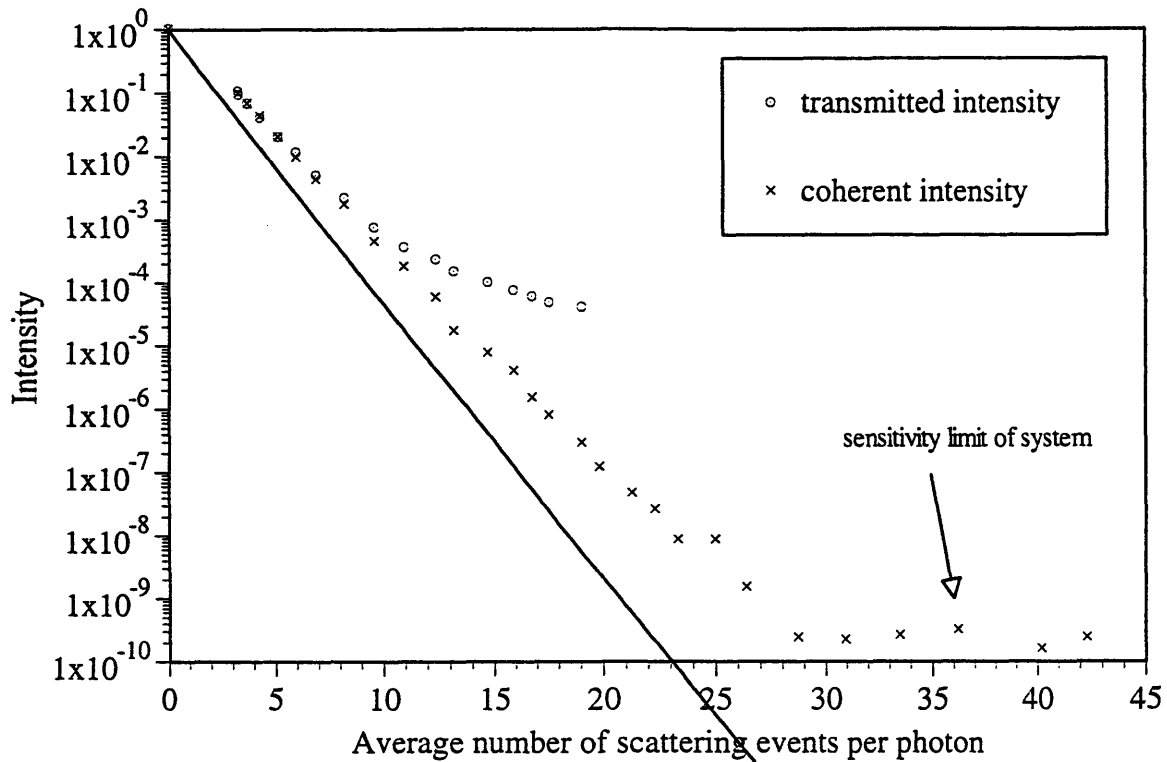
Figure 2.10: Plot of the normalized coherent light intensity versus the average number of scattering events within the turbid medium for each photon. This experiment is done with the AOM set-up in the signal beam arm. In this case, the sensitivity limit is imposed by the presence of power fluctuation of the laser.

In conclusion, we have explained in detail the heterodyne experiment set-up and the relevant equations required for our experiment. The next chapter will elaborate on the experimental data that we obtained.

Chapter 3

Experimental Result

As mentioned in the introduction, isolating the forward-scattered light from the incident light beam is a significant problem for any experiment designed to measure the coherence of forward-scattered light. There are two approaches for resolving this problem. The first approach is to temporally resolve a transmitted laser pulse. The other approach is to collect only the portion of transmitted light which has been deflected by a small angle from the direction of the incident beam.

For the first approach, due to slight alterations in the direction of propagation from scattering, a photon which is scattered a few times will follow a longer path through the media than an unscattered photon. As a result, scattered photons tend to arrive later at the detection system than unscattered photons (ballistic photons). By temporally gating the transmitted pulse, we can therefore extract only the component of light which has been scattered. Fujimoto's group at MIT adopted this approach to study coherence in scattered light [7]. The experiment involved sending a stream of 50 fs laser pulses through a turbid medium, temporally gating the transmitted light and measure its coherence via a heterodyne setup. With such, they detected photons which preserve coherence after having experienced 20 - 50 scatterings. The drawback of this scheme is that it is unable to resolve photons which have been scattered only a few times from ballistic photons because these scattered photons follow paths through the medium which

are extremely close to that of ballistic photons and hence will arrive at the detector at nearly the same time as ballistic photons.

There is another issue involved in the mentioned experiment by Fujimoto's group. The signal beam is arranged to diverge before it enters the turbid medium. The transmitted beam is then refocused into a receiving fiber optics. This initial divergence makes it difficult to create a reasonable model for the analysis of results.

The second approach is the one we adopt for our experiments. In this case, if we select an appropriate off-axis angle to detect the transmitted light at, we would be able to isolate photons which are scattered only once from the ballistic photons. The challenge in this approach is the difficulty in matching the direction of the reference beam at least roughly to the direction of these scattered photons so that we get a maximal interference pattern. We had some success in doing this and our methodology shall be presently elaborated. In addition, we shall present the relevant experimental data that have been obtained.

3.1 On Axis Experiment

3.1.1 Experimental Details

In the first set of experiments, no spatial angular displacement is used. The experiment is done by collecting the transmitted light at the center of the bulls eye interference pattern. This set of experiments serves as a verification of the Mie Theory [7] and a calibration of our system.

The initial alignment of the system to obtain a good heterodyne signal is as detailed in scetion 2.2. Having thus aligned and calibrated the system, we then insert a

dense solution of Polysciences polystyrene microspheres. These microspheres have fairly constant diameter with respect to each other. This uniformity permits us to treat the spheres as being practically identical for the purpose of calculating their scattering cross-section, σ_s, and the anisotropic scattering factor, g, from Mie scattering theory [8].

In most of these experiments, the diameter of the aperture is 560 microns and the aperture and photodiode array subtends a solid angle of 6.3×10^{-6} steridian centered on the signal beam. These values are selected to collect all the light within the bulls eye interference pattern center spot so that the heterodyne signal is maximized. In one particular experiment, however, we tried a smaller aperture of 420 microns, which gives a corresponding solid angle of 3.5×10^{-6} steridian.

These aperture sizes are accurate to within 5% of the given values. Their diameters cannot be determined by direct measurement due to the smallness of the aperture and the location of the aperture on its mounting. We are able to ensure accurate aperture size by inserting drill bits of known size into the aperture and closing it around the drill bit. When the aperture is fully close on the drill bit, we can be certain the aperture size is equal to the diameter of the drill bit.

We can compute the average number of scattering events each photon will experience as it traverses the medium by equation (2.1) with the knowledge of σ_s, the number density of the solution, n, and the length of the container which is equal to 2.6mm.

We record the intensity of the transmitted signal beam by blocking the reference beam and measuring the signal beam with the photodetector. We repeat this measurements at various concentrations of the microsphere solution. By doing so, we can profile the transmitted intensity over a density range which produces average scattering events which typically ranges from 0 to 40.

The coherent intensity of the transmitted light is profiled in a similar approach. Except, in this case, we allow the reference beam to combine with the transmitted signal beam. The resulting heterodyne amplitude is measured and it can be substituted in equation (2.8) to yield the coherent intensity of the transmitted light.

We use various microsphere diameters in our experiment, they include microspheres of diameter: 1.072 μm, 4.33 μm, 10.568 μm and 22.01 μm. Their respective Mie theory predicted scattering cross-sections at the laser wavelength of 753nm are: 1.90×10^{-8} cm^2, 3.36×10^{-7} cm^2, 2.01×10^{-6} cm^2 and 7.59×10^{-6} cm^2.

3.1.2 Experimental Data

Fig. 3.1 - 3.4 shows the experimental data obtained in this series of experiments. Fig. 3.5 shows the reproducibility of an experiment with two separate preparations of the microsphere solutions. Also shown on each curve are the normalized transmitted intensity and the computed coherent intensity extracted from the heterodyne signal amplitude.

As we mentioned before, we detect the transmitted light centered on the input beam in this set of experiments. The transmitted intensity is dominated by the ballistic component for an average number of scattering events ranging from 0 to about 8 as can be seen from the experimental data. This is reasonable, as scattering events will most likely deflect photons away from the center of the signal beam. As the average number of scattering events increases to about 8 - 10, we start to see a rise in the proportion of the scattered component, as indicated by the change of the transmitted intensity slope. This is predictable because the ballistic component of the light is attenuated as an exponential function of the average number of scattering events. On the other hand, multiple scattering events eventually return some of the photons to the central beam path. This prediction is consistent with Fig. 3.2 where a smaller collection angle is used. In such a
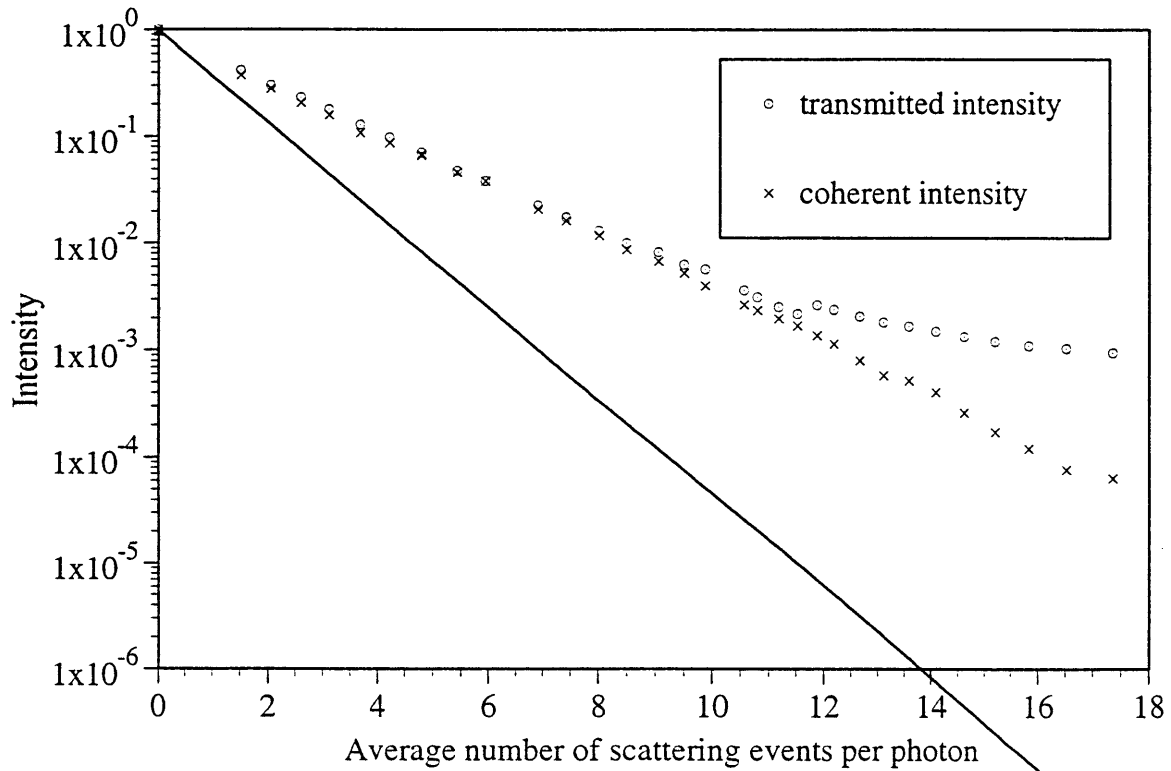
Figure 3.1: Plot of the measured intensities versus average number of scattering events per photon, $\overline{Z}_s$, for 1.072 μm wide microspheres. The solid line is the predicted exponential attenuation curve for the ballistic intensity based on Mie theory predicted cross section of 1.90×10^{-8} cm^2. Experiment is done with a collection angle of 6.3×10^{-6} steridian centered on the transmitted beam.
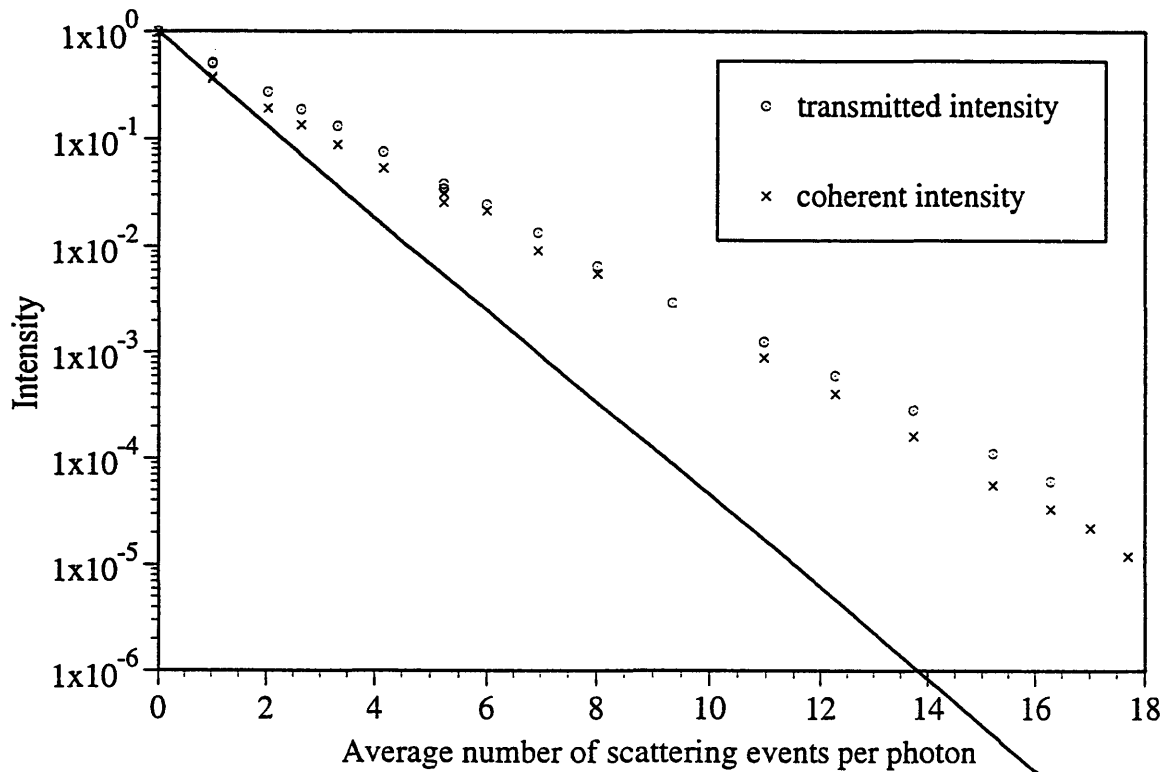
Figure 3.2: Plot of the measured intensities versus average number of scattering events per photon, $\bar{Z}_s$, for 4.33 μm wide microspheres. The solid line is the predicted exponential attenuation curve for the ballistic intensity based on Mie theory predicted cross section of 3.36×10^{-7} cm^2. Experiment is done with a collection angle of 3.5×10^{-6} steridian centered on the transmitted beam.
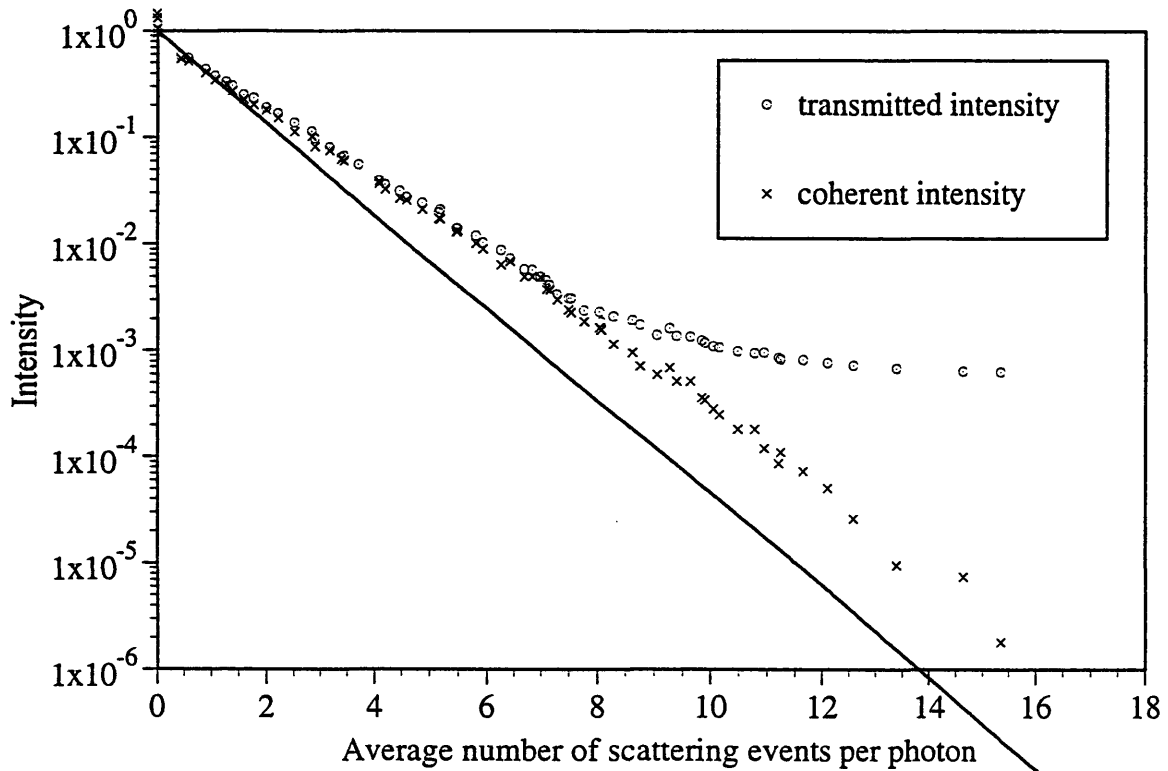
Figure 3.3: Plot of the measured intensities versus average number of scattering events per photon, $\bar{Z}_s$, for 10.568 μm wide microspheres. The solid line is the predicted exponential attenuation curve for the ballistic intensity based on Mie theory predicted cross section of 2.01×10^{-6} cm^2. Experiment is done with a collection angle of 6.3×10^{-6} steridian centered on the transmitted beam.
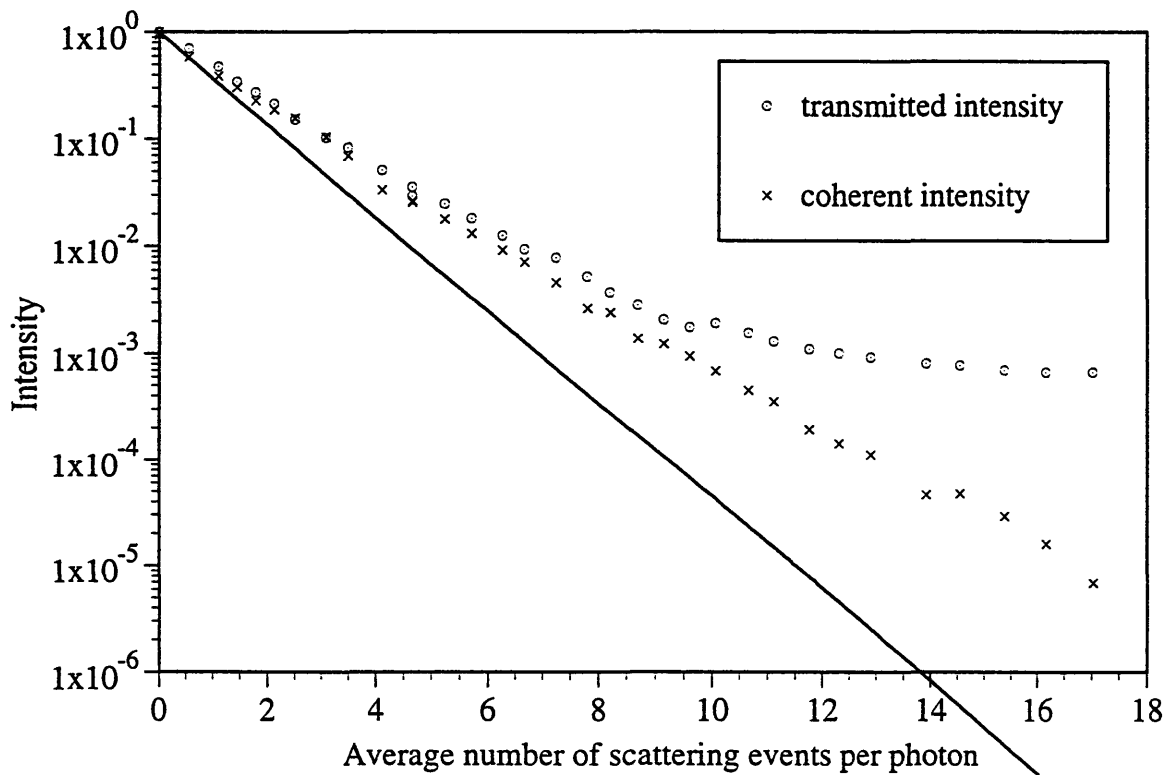
Figure 3.4: Plot of the measured intensities versus average number of scattering events per photon, $\overline{Z}_s$, for 22.01 μm wide microspheres. The solid line is the predicted exponential attenuation curve for the ballistic intensity based on Mie theory predicted cross section of 7.59×10^{-6} cm^2. Experiment is done with a collection angle of 6.3×10^{-6} steridian centered on the transmitted beam.
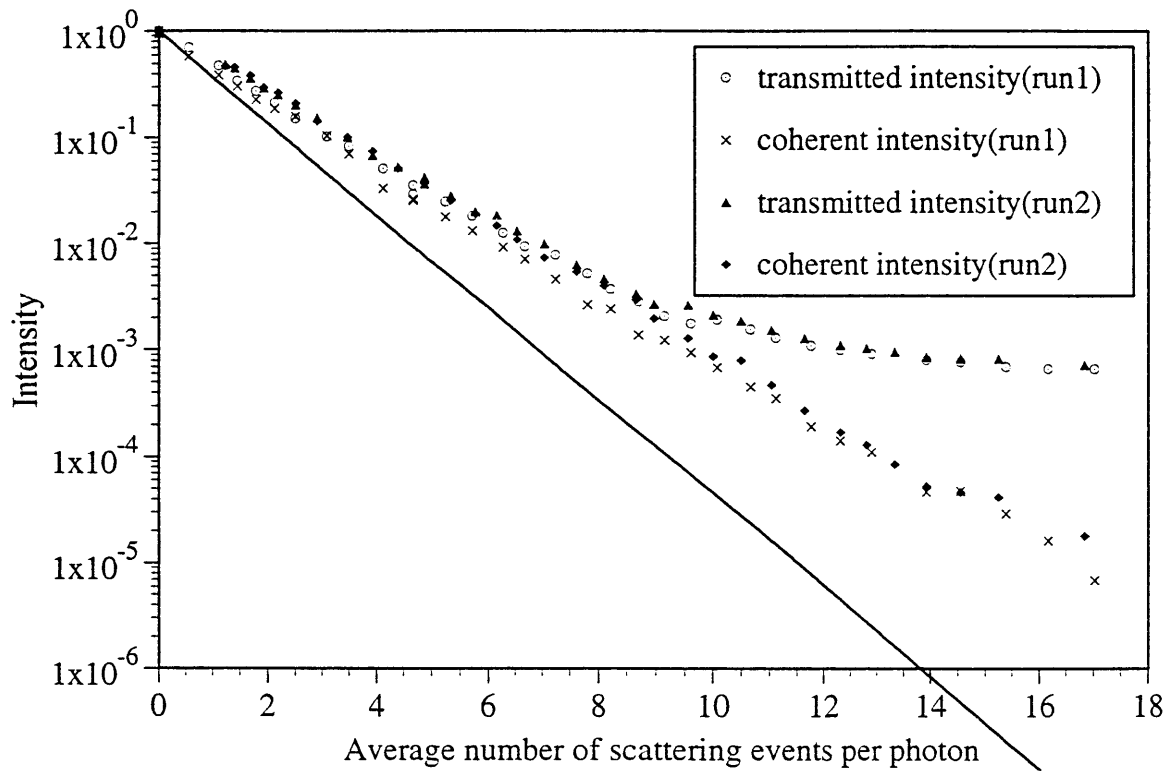
Figure 3.5: Plot of the two separate runs of the same experiment shows consistency. The plots are for measured intensities versus average number of scattering events per photon for 22.01 μm wide microspheres with Mie theory predicted cross section of 7.59×10^{-6} cm^2. Experiment is done with a collection angle of 6.3×10^{-6} steridian centered on the transmitted beam.
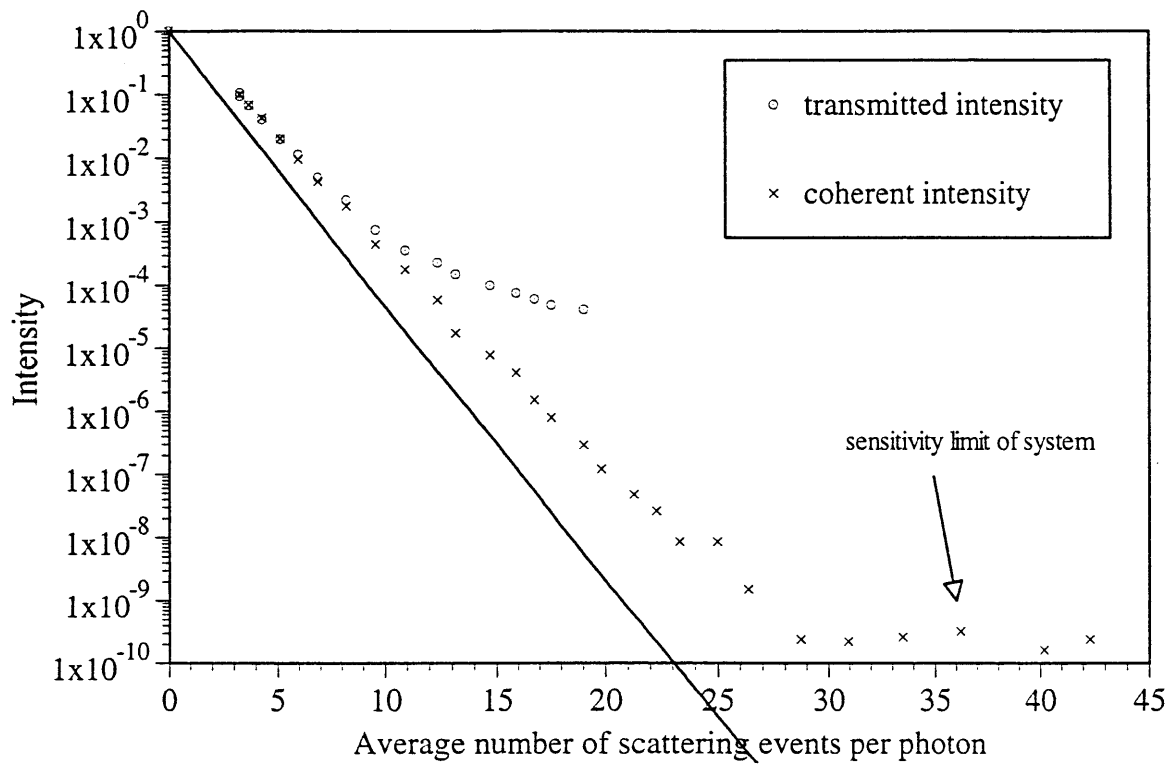
Figure 3.6: An extended plot of the measured intensities versus average number of scattering events per photon for 10.568 μm wide microspheres with Mie theory predicted cross section of 2.01×10^{-6} cm^2. Experiment is done with a collection angle of 6.3×10^{-6} steridian centered on the transmitted beam.

situation, more scattering is required before some of the photons return to the more narrowly defined collection direction. As such, we should see the dominance of the ballistic component for a wider range of average number of scatterings than for those experiments done with larger collection angle.

Also included in the experiment plots are the attenuation curves for the ballistic component of the light, assuming the scattering cross sections are as given by the Mie theory. As can be seen from the figures, there is a discrepancy between the theoretical prediction and the experimental result. The experiments indicated scattering cross sections which are 50 - 70% smaller for the microspheres. It is worth noting that the cross sections are very sensitive to the refractive indexs involved. An error of 0.002 in either the refractive index of the water or the microspheres can alter the computed cross sections by about 8%. However, the observed discrepancy is much too large to be accounted by such. Given the consistency of our experiment over separate runs, we believe the error lies in our application of Mie theory. The problem is as yet unresolved but is not crucial to the rest of the analysis presented here.

It can be seen on all the figures that the coherent intensity matches up with the transmitted intensity at the earlier part of the plots. This is consistent with our observation from the behavior of the transmitted intensity alone, specifically that the transmitted intensity is dominated by the ballistic component of light until a gradient change occurs. Since ballistic light is wholly coherent, we naturally expect the coherent intensity measurement to match up with the transmitted intensity curve at the beginning.

When the transmitted intensity starts showing a significant component of scattered light, as indicated by the gradient change, we observe a deviation of the coherent intensity from the transmitted intensity on the plots. The coherent intensity curves continue their effectively exponential drops with larger average number of scattering events, while the transmitted intensity curves decrease more gently. Fig. 3.6 shows the good conformity of this decrease in the coherent intensity over a wider range of average number of

scatterings; no change in gradient as seen with the transmitted curve is observed for the coherent intensity curve. This suggests that, in this configuration, the coherent intensity is dominated by the ballistic component which also has an exponential relation to the average number of scattering events.

Conceivably, if we are able to attenuate the ballistic component of the light even further by increasing the average number of scattering events, the coherent intensity might start to show some gradient change indicating the presence of coherent scattered light. Indeed, Fujimoto's group demonstrated that if the ballistic component is attenuated sufficiently, coherent scattered light would start to show up in the measurements [6]. The issue involved with such an experiment is that the coherent scattered light would be made up of photons which have been scattered many times. A theoretical analysis of these photons will be complicated.

Our experimental set-up should allow us to detect such coherence, The improvement required to do so is the refinement of our detection scheme to achieve shot noise limited detection of the light intensity. Doing so will further extend the sensitivity of our system by 35 dB, thereby permitting us to easily detect this coherent scattered light which is at a power level of about 120 dB below the initial incident intensity.

There are two factors in this type of experiments which make it difficult to detect coherent scattered light. First, the strong ballistic component of the beam prevents us from detecting scattered component until we reached an average number of scattering events per photon of about 8. At that point, the signal is relatively weak and the observed scattered photons would have undergone many scattering events. Second, the system is optimized by the choice of the collection solid angle and the alignment along the signal path direction, in order to optimize for the observation of heterodyne signal from the ballistic photons and scattered photons which are traveling in almost the same direction and which exhibit wavefronts that are similar to those ballistic photons. If the scattered light should exhibit a non-uniform wavefront then the heterodyne signal that can arise

from the scattered light may very well be washed out when averaged over the detection area of the aperture and photodiode arrangement. This problem can be minimized by using a detector collection area which is smaller than the fringe width and the size of non-uniformity of the scattering wave front. Reducing the collection area leads to its own problem; the signal will no longer be large and detection will be difficult.

3.2 Off Axis Experiment

3.2.1 Experimental Details

It is with these two consideration in mind that we decided to do the following set of experiments. The alteration made to the existing experiment is that we tilt the incoming signal beam slightly (about 5 mrad) before it enters the turbid medium (see Fig. 3.7).

By tilting, we effectively cause the signal beam to no longer fall directly on the detection area. Due to the gaussian beam profile of the laser, we still collect a portion of the ballistic light. Depending on the angle of tilt, we can have less than one thousandth of the ballistic light making it to the detector, as compared to when the beam is centered on the detector.

We performed an experiment to verify the profile of the signal beam. In this experiment, we moved the aperture across the width of the signal beam. This is equivalent to tilting the signal beam; the micrometer gauge that is already mounted on the aperture makes measurement of the angular displacement an easier experiment to do. The aperture is about 25 cm from the center of the glass container of turbid medium. In the situation where we have water in the container, the beam profile can be effectively mapped out as shown in Fig. 3.8. As we can see, it is possible to get less than one

thousandth of the original beam to fall on the detector by setting the detector's collection area more than 10 mrad off the signal beam direction.

This reduction of the ballistic component incident on the detector makes it easier to detect scattered light when the average number of scattering in the turbid medium is small. The reason is the following. The majority of scattering occurs at the center of the beam where the intensity is the greatest. Even a small portion of the scattered light from that central region when scattered into the detector area can dominate over the incident ballistic component.
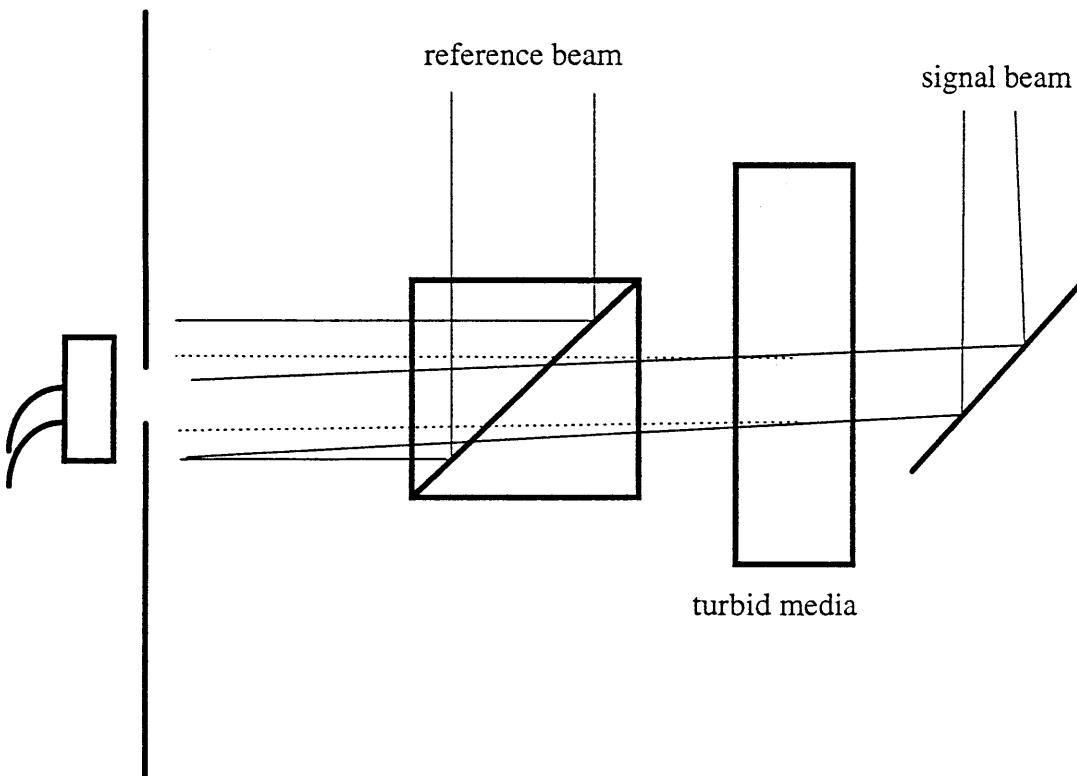
Figure 3.7: Sketch of the altered experiment where the signal beam is no longer falling in the center of the aperture. The amount of ballistic light incident on the collection area is thus reduced so that even a small amount of scattered light can now be detected.

As can be seen from the experimental data on Fig. 3.8, the turbid medium serves to scatter light away from the central region and creates a stronger intensity profile at an

angle off the center. The prediction is further confirmed by the higher off-center intensity from the experiment with a denser turbid medium; more scattering will scatter more light away from the central region while redistributing more light at small angles from the center.
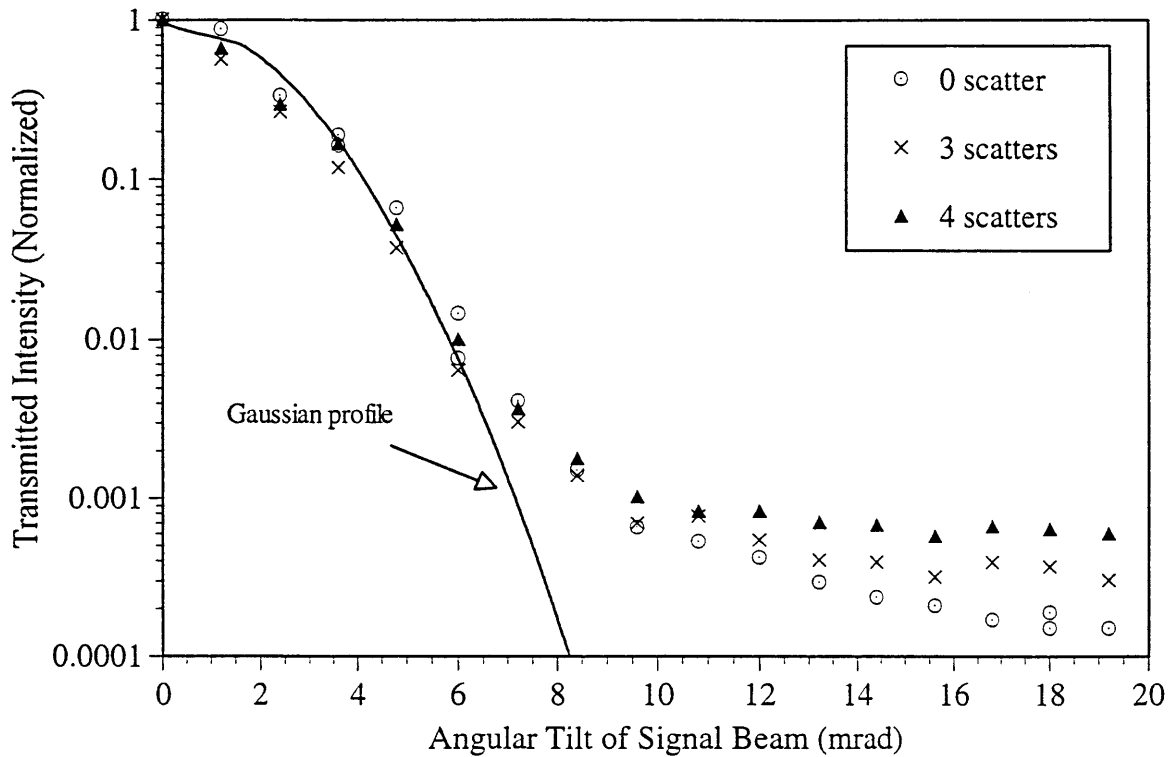
Figure 3.8: Experimental data showing the intensity profile of the signal beam. Notice that scattering events serve to even out this profile. The deviation from a true Gaussian fit suggests our laser beam's profile is altered by diffraction effect due to the finite size of the optical components used in the experiment.

Besides decreasing the ballistic component incident on the detector area and making it easier to detect small amounts of scattered light, this arrangement also show less of an optimization for the detection of heterodyne signal from the ballistic photons. More specifically, because the signal beam direction is no longer parallel to the reference beam direction, the bulls eye interference pattern we had before is now replaced by a fringe pattern. At a 20 mrad tilt of the signal beam, we get about 5 fringes across the detection area. These fringe patterns tend to average out so that the net heterodyne signal

is smaller than previous. On the other hand, as can be seen from Fig. 3.7, the scattered light that falls on the detection area will be comparatively more parallel to the reference beam path. This implies that the interference pattern formed by coherent uniform wavefront scattered light with the reference beam will be a bulls eye interference pattern or wider fringe patterns. In terms of the $a(A,\theta\ (x,y,t),\Delta\omega)$ factor, it will be smaller for the ballistic light and larger for the scattered light.

3.2.2 Experimental Data

For this set of experiments, we used 4.329 μm wide polystyrene microspheres. The aperture size was also reduced to 420 μm in an attempt to reduce area dependent averaging off of the heterodyne signal mentioned earlier. The experiment begins by the alignment of the signal beam with the reference beam until a bulls eye interference pattern is obtained with water in place of turbid medium. The signal beam is then tilted by small known angle. The $a(A,\theta\ (x,y,t),\Delta\omega)$ is next determined in the same manner as detailed previously. We should keep in mind that scattered light's $a(A,\theta\ (x,y,t),\Delta\omega)$ is likely to be different from this $a(A,\theta\ (x,y,t),\Delta\omega)$ found for the ballistic light.

The turbid medium is then added and diluted incrementally. Measurements of the transmitted light and the heterodyne amplitude are made in the same manner as specified previously. These scans across various concentration of the turbid medium are done for angular tilts of 0, 4, 10, 12 and 20 mrad. Fig. 3.9 - 13 shows the intensity plots for these experiments. Fig. 3.14 shows the compiled transmitted plots for all angular tilts and Fig. 3.15 shows the compiled coherent intensity plots.

It can be seen from Fig. 3.14 that the decline in the transmitted intensity is more gradual for tilt angles. This is consistent with what we have said so far. At reasonably large tilt from the signal beam direction, the initial incident ballistic component is small.

Addition of turbid medium reduces this component but, at the same time, scatters a significant proportion of light from the center of the beam onto the detection area. At smaller tilt angle, the initial incident ballistic component is large. The contribution of an additional scattered component is insignificant even when this initial ballistic component is attenuated by the turbid medium. In all the cases, the decrease of the ballistic component is an exponential of the average number of scattering events. As discussed in Sec. 3.1.2, the near exponential decrease in the transmitted intensity of the experimental curve for no angular tilt profiles the attenuation of the ballistic component over the average number of scatters. With this in mind, we can easily see from the deviation of all other curves from the one for no angular tilt that there are significant proportions of scattered light even when there are only 1 or 2 scattering events per photons on average; we can detect the presence of photons which are scattered only a few times in this set of experiment.

The coherent intensity plotted in 3.9 - 13 and 3.15 are obtained, as before, by applying the heterodyne signal amplitude, the reference beam intensity and $a(A,\theta\ (x,y,t),\Delta\omega)$ found initially into equation (2.8).

If the assertion in conventional theories that scattered photons preserve no coherence is true, then all of these coherent curves should match up with the exponential attenuation profile of the ballistic light component. This is clearly not the case here; except at no angular tilt, all the other angles results in curves which are above the ballistic attenuation prediction. This deviation implies that some of the scattered photons are coherent and lead to this increase in observed coherent intensity.

There are two features in the experimental result which we would like to point out before we present a theoretical model to explain this deviation. The first is our observation that the heterodyne signal amplitudes in these set of experiment fluctuate slowly on the time scale of 0.1 - 1 s. The fluctuation is large enough that the computed coherent intensity at one point in time can be up to 3 times higher than at another point. In
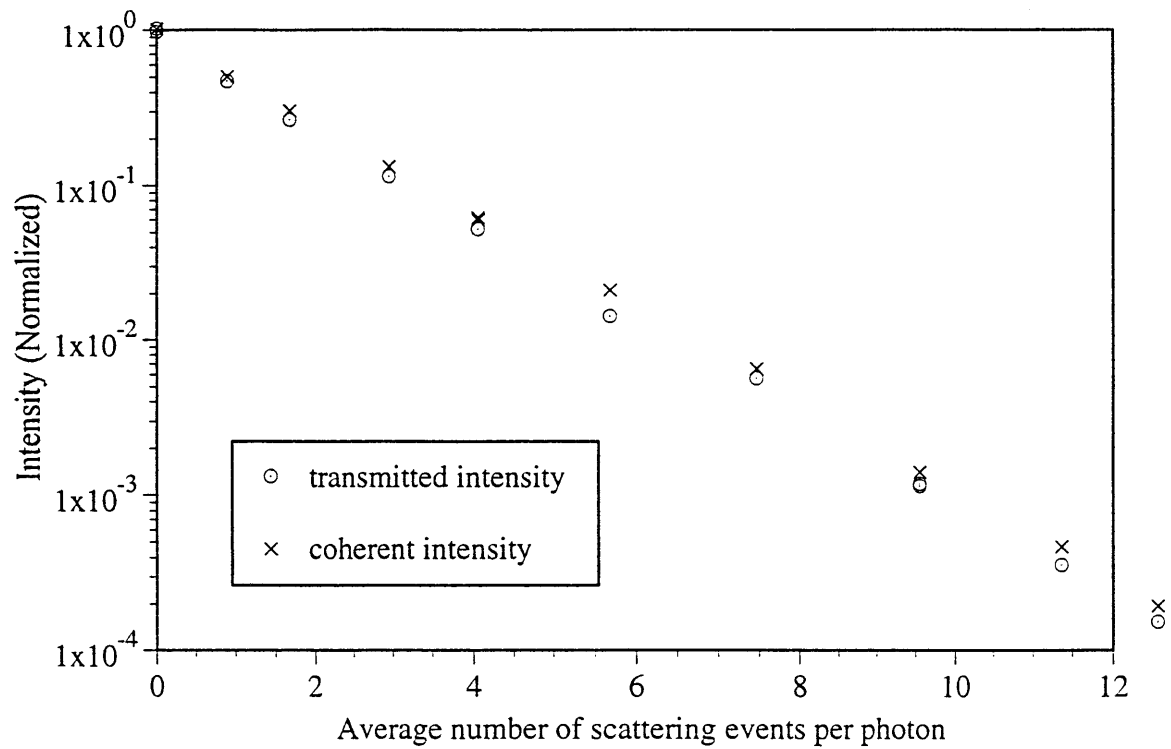
Figure 3.9: Plot of the measured intensity curves for a signal beam tilted by 0 mrad from the reference beam.
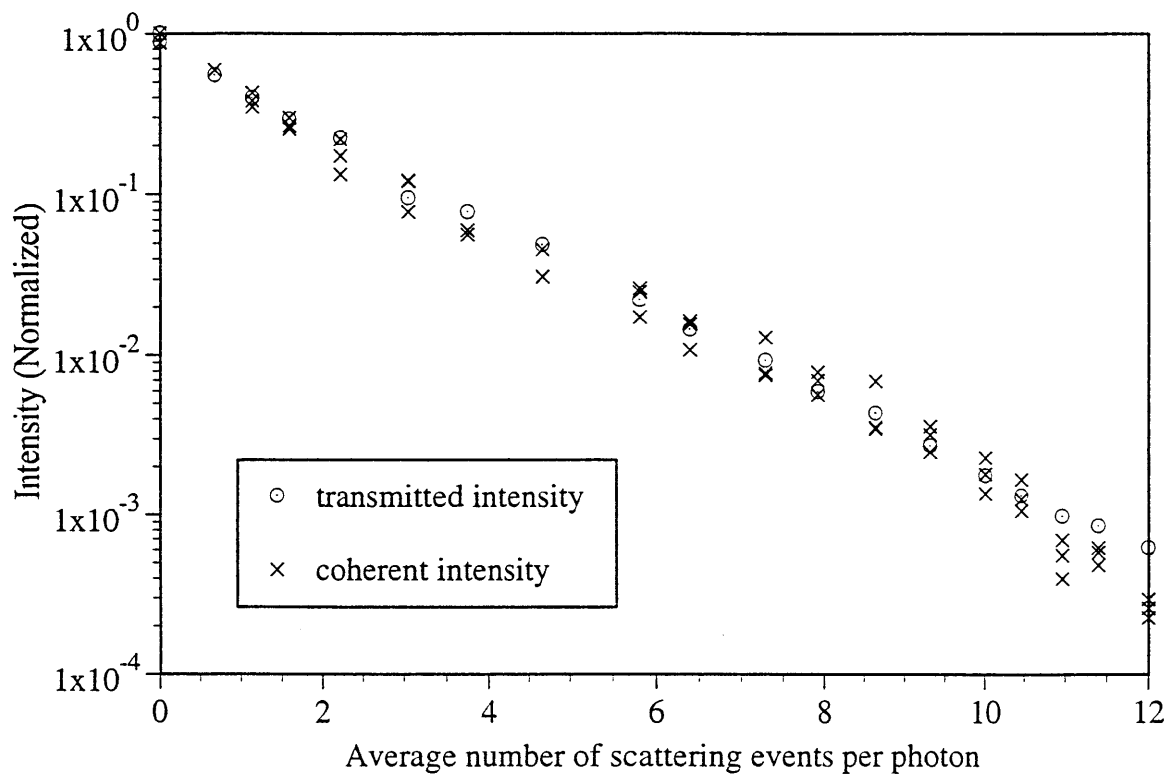
Figure 3.10: Plot of the measured intensity curves for a signal beam tilted by 4 mrad from the reference beam.
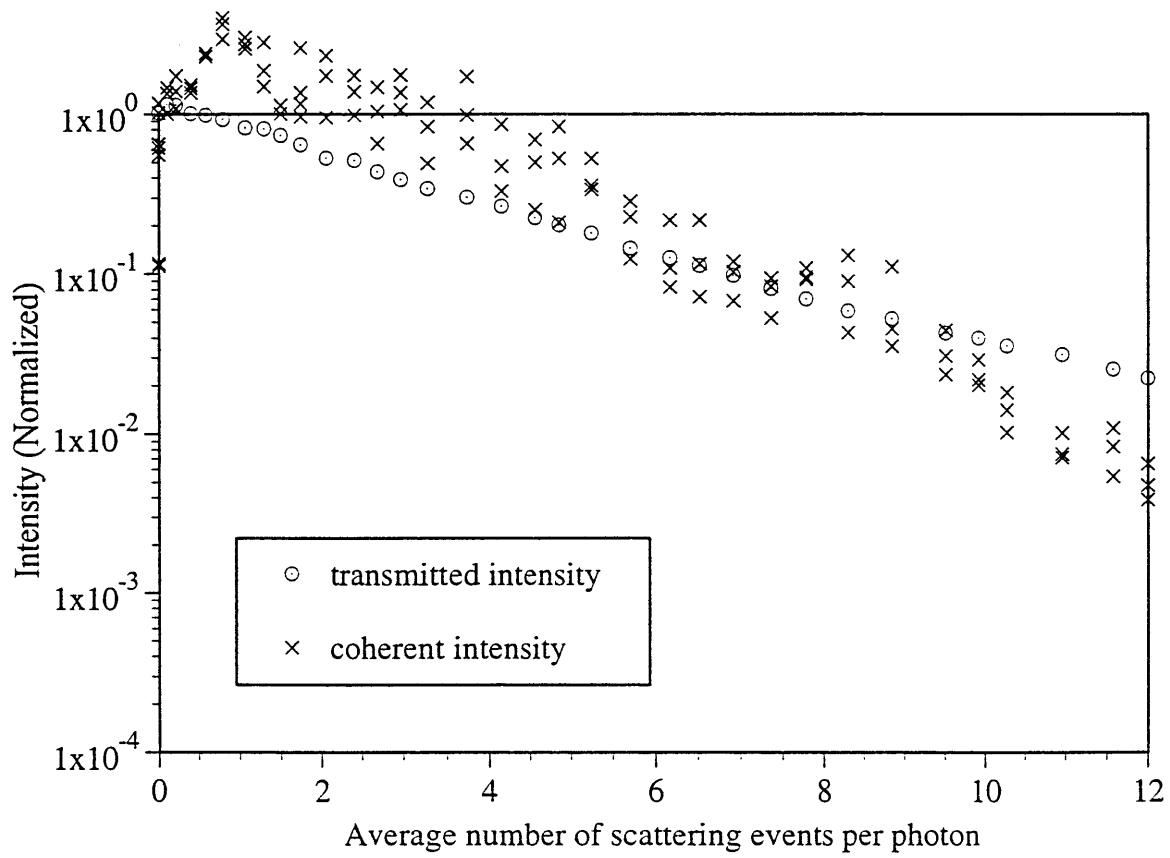
Figure 3.11: Plot of the measured intensity curves for a signal beam tilted by 10 mrad from the reference beam.
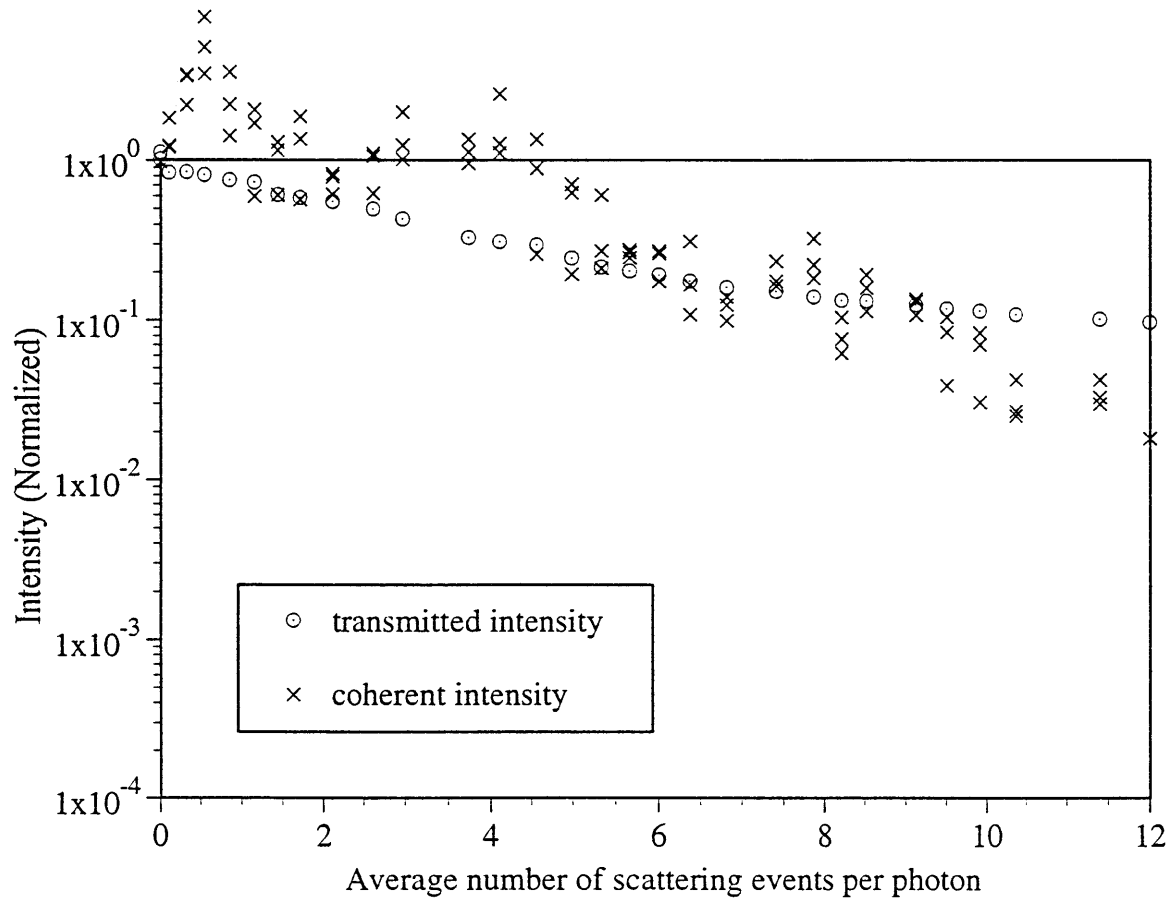
Figure 3.12: Plot of the measured intensity curves for a signal beam tilted by 12 mrad from the reference beam.
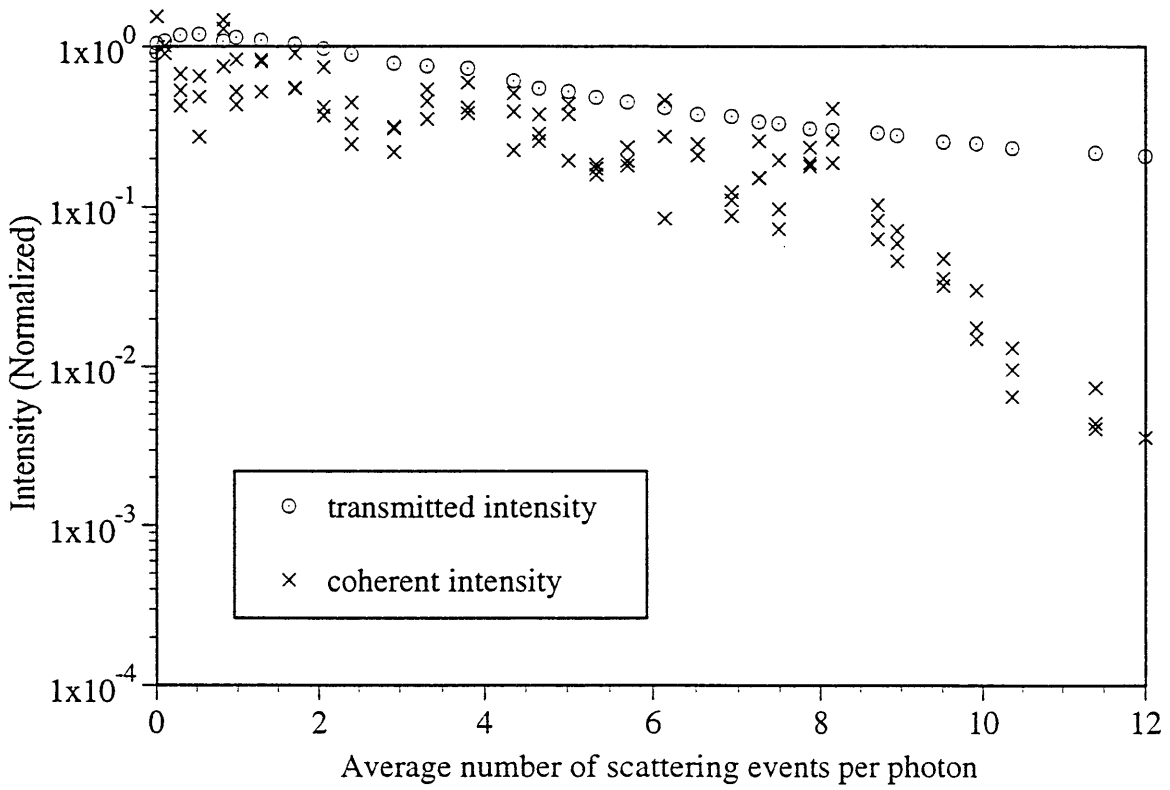
Figure 3.13: Plot of the measured intensity curves for a signal beam tilted by 20 mrad from the reference beam.
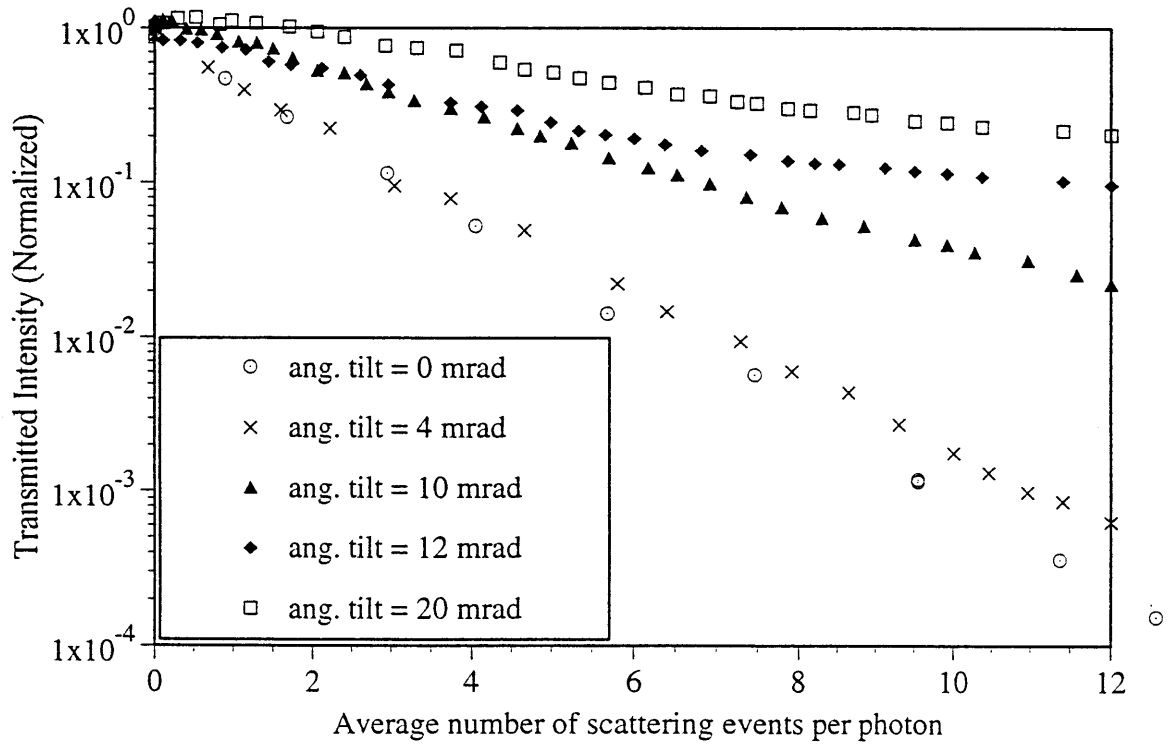
Figure 3.14: Plot of the measured transmitted intensity curves.
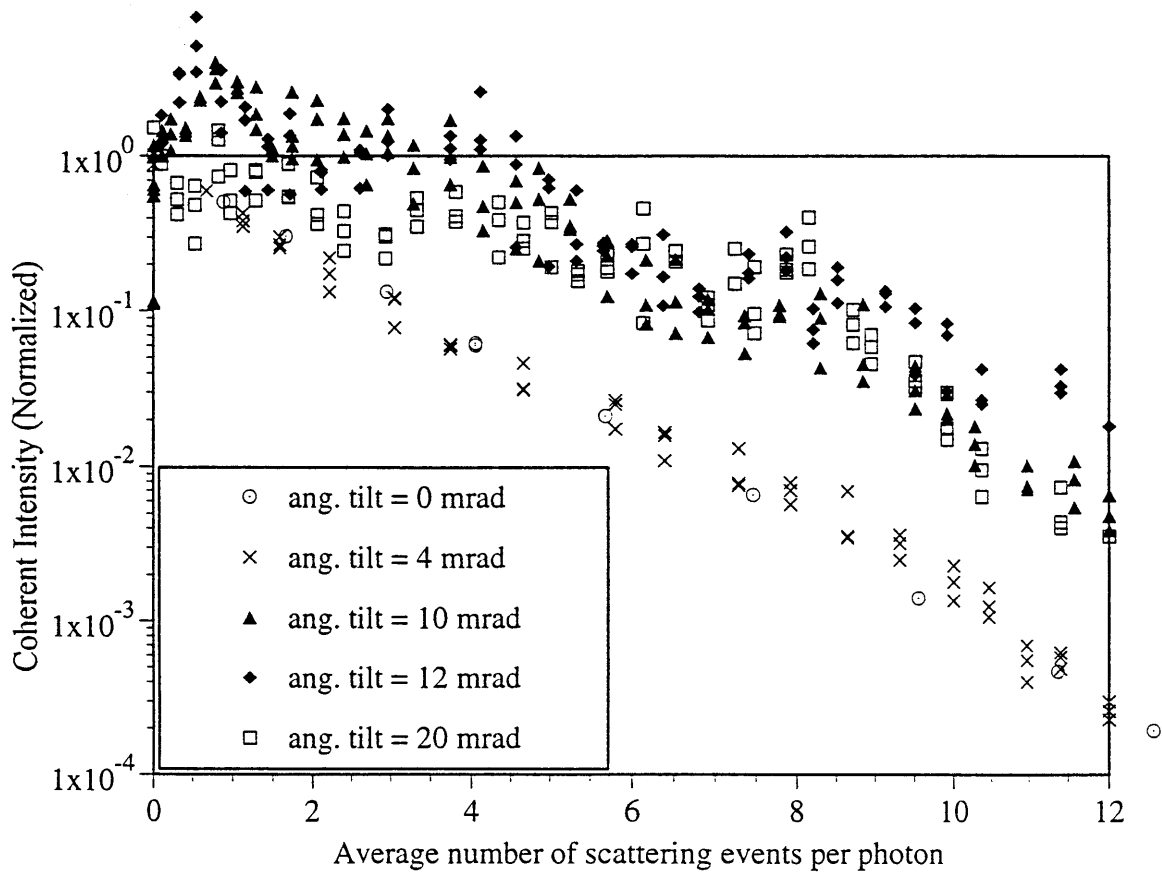
Figure 3.15: Plot of the measured coherent intensity curves.

our experiment, we tried as far as possible to record these variations by taking 3 measurements at each point of the experiment. A qualitative explanation of this fluctuation shall be deferred until we elaborate on the theoretical model.

The second point which we would like to bring up at present is the observation that the coherent intensity curves at 10 and 12 mrad exceed the transmitted intensity curves in some ranges. This is not possible realistically because the transmitted intensity should be a measure of the total intensity, of which the coherent intensity a fraction. The mystery is deepened by the behavior of the curve made at 20 mrad, which shows no such violation.
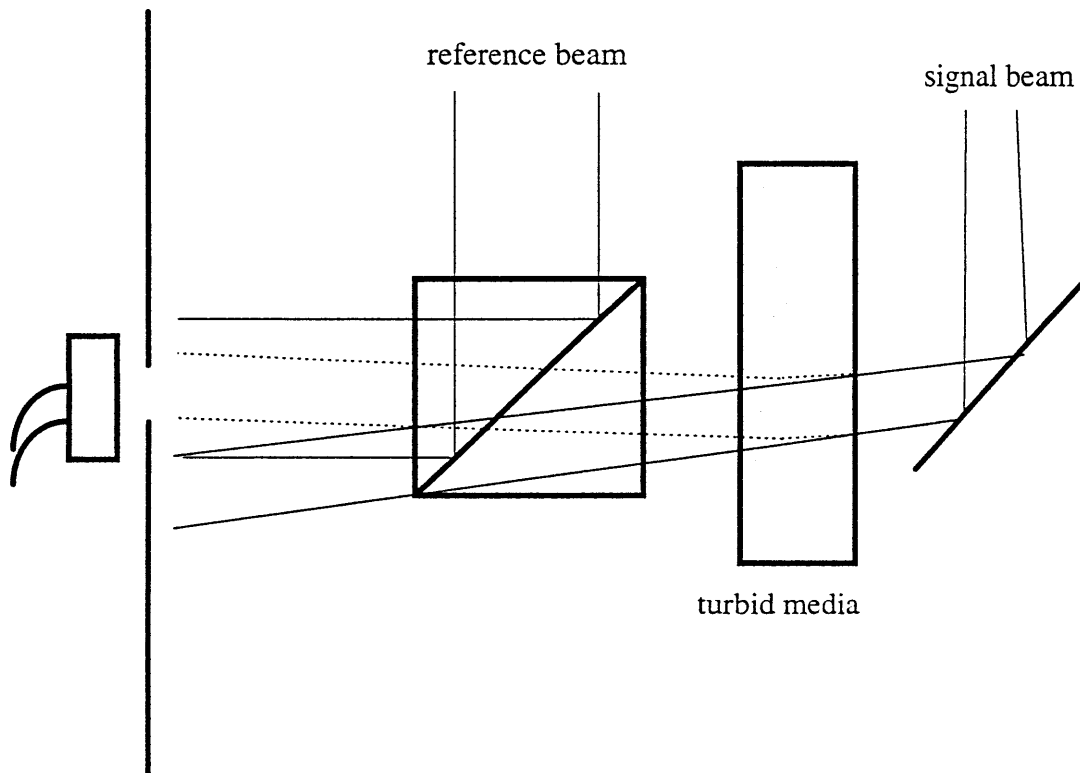
Figure 3.16: Sketch of the experiment with the signal beam at a relatively large angular tilt from its original alignment with the reference beam. In this case, the scattered photons which arrive at the detection area have to bend a significant amount and are no longer near parallel to the reference beam.

It turned out that this phenomenon can be readily explained by remembering that the coherent intensity curves we plotted here are obtained with the use of $a(A,\theta\,(x,y,t),\Delta\omega)$ found at zero scattering with ballistic light. As mentioned above, $a(A,\theta\,(x,y,t),\Delta\omega)$ is likely to be larger for the scattered light as it is more along the direction of the reference beam. Put in simple terms, scattered light compared to ballistic light will show a larger heterodyne signal amplitude for the same amount of coherent light. If we compute the amount of the coherent light by using the signal amplitude and $a(A,\theta\,(x,y,t),\Delta\omega)$ for both, the computation will give an overestimation for the scattered light.

The observation that such overestimation is less in the 20 mrad tilt experiment can be explained by realizing that at large angular tilt, the scattered photons that arrive at the detection area must bend their original optical path significantly. This causes the scattered light to have a significant angular deviation from the reference beam, as shown in Fig. 3.16. This results in $a(A,\theta\,(x,y,t),\Delta\omega)$ being smaller for the scattered photon, hence possibly eliminating the overestimation problem or at least mitigating the problem to some extent.

In summary, we demonstrated the observation of coherence in photons which are scattered a few times in this set of experiments. This experimentally proves that the assumption that scattered photons preserve no coherence is a theoretical simplification rather than an experimental fact. In the next chapter, we shall explain a qualitative model that can be applied to these experimental results.

Chapter 4

Theoretical Analysis.

The objective of this theoretical analysis is to provide a qualitative framework for understanding the observed preservation of coherence in scattered photons. The conventional models, where coherence is assumed totally lost in scattering has been experimentally shown to be inaccurate; it is necessary that a more physically correct model be developed. We shall first list the features of the experimental results obtained so far, which a well-formed and physically correct theory should be able to account for and explain. We then look at two very simple models and point out their respective shortcomings. Next, a qualitative model based on the non-uniformity of the scattered wavefront is presented. We then examine this model and see if the mentioned experimental features will be manifested in this model.

4.1 Observed Behavior of the Coherent Scattered Light

There are three features in the data from the tilted signal beam experiments presented in the previous chapter that are consistently observed in all the experiments. Since these features are manifested only in experiments where the coherent scattered

component is measurably significant, it is reasonable to expect that they are related in some way to the nature of the coherent scattered light.

The first of these features is that the measured coherent component is always larger than the ballistic component. Specifically, in Fig. 3.15, we can take the coherent component curve at zeo angluar tilt to depict the exponential attenuation profile of the ballistic component with increasing average number of scattering events; it can be seen that all the other curves in the same figure are higher at all points than the ballistic profile. In all those curves, we know from the transmitted intensity measurements that the scattered component is comparable or larger than the ballistic component over most of the range. This observed positive deviation from the ballistic profile should therefore be somehow related to the presence of coherent scattered light.

An erroneous explanation of this behavior would be to assert that the coherent component is made up of the sum of the ballistic intensity and the coherent scattered intensity. Therefore, the coherent intensity profile is necessarily higher than the ballistic intensity. This is incorrect because if the scattered light has some coherence, we would need to add the electric fields from the ballistic and scattered component to get a total electric field. The intensity derived thus is not a simple sum of intensities. A good illustration of this can be found in the following example. Suppose we have a situation where the coherent scattered component is propagating in the same direction as the ballistic component; in addition, they are exactly equal in magnitude and in phase with each other. In such a case, the resulting measured coherent intensity will be twice higher than if we simply added the two intensities together.

The second feature is that the experimental result suggests that the coherent intensity profile deviates from the transmitted intensity profile. Recall from Chapter 2 that the coherent intensity profile is computed from the heterodyne signal amplitude and the $a(A, \theta\,(x, y, t), \Delta\omega)$ factor by (2.8). As mentioned in Chapter 4, the $a(A, \theta\,(x, y, t), \Delta\omega)$ factor is different for ballistic light and coherent scattered light due to the geometry of the

problem. As such the effective $a(A,\theta\,(x,y,t),\Delta\omega)$ is likely to change as the average number of scatters varies, the computed coherent intensity profiles in Fig. 3.9 - 13 and 3.15 are therefore distorted to some extent by this. However, we can still extract useful information about the true coherent intensity profile by focusing our attention at the region where the ballistic component is negligible due to attenuation and where the scattered component is dominant.
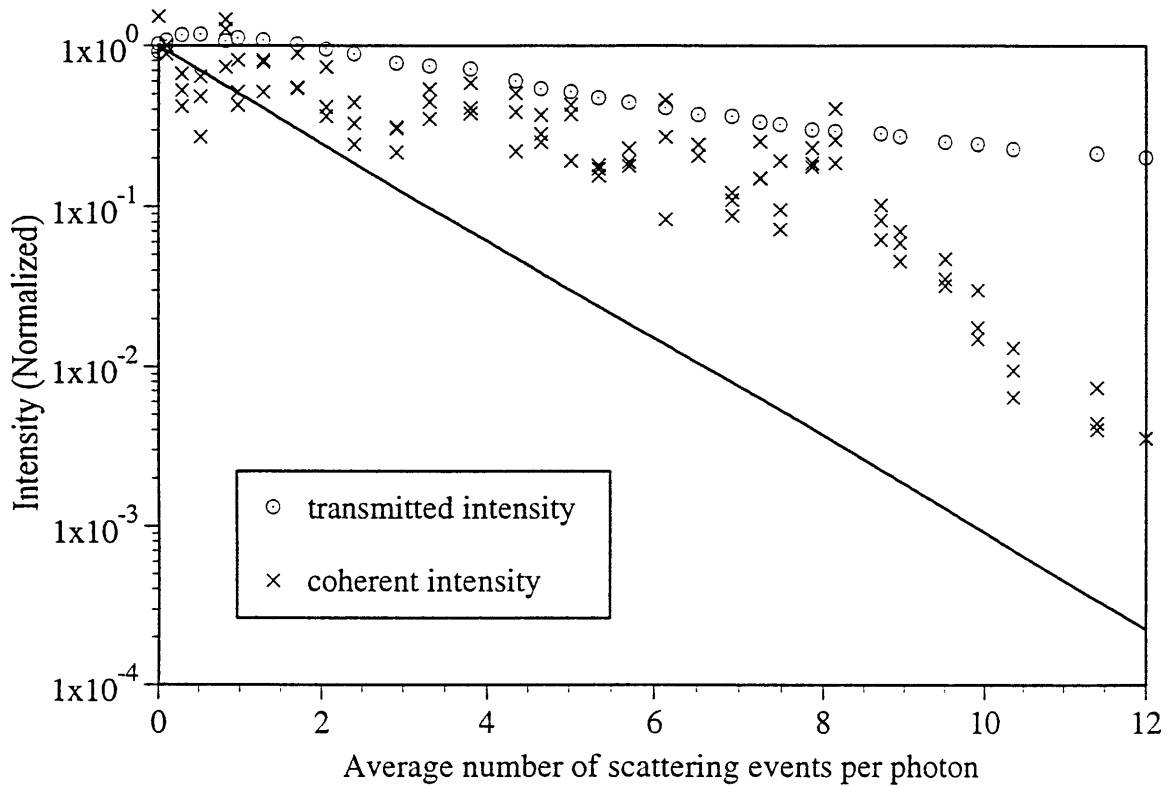
Figure 4.1: Plot of the measured intensity profiles for a signal beam tilted by 20 mrad. The ballistic intensity profile depicted here is derived from the experimental data form the no angular tilt experiment.

Take for example, the experimental result shown in Fig. 3.13 reproduced here as Fig. 4.1. Notice that in the range where the average number of scattering events is larger than 8, the observed transmitted intensity is at least 2 orders of magnitude larger than the ballistic component intensity, this indicates the amount of gathered light is predominantly scattered light. Over this range, we would therefore expect $a(A,\theta\,(x,y,t),\Delta\omega)$ to take on

a constant value, namely the value for scattered coherent light. In this case, the gradient of the computed coherent intensity profile should be accurate. The difference in this gradient from the transmitted intensity gradient implies that the two curves are different. Since the total transmitted intensity is a sum of coherent and incoherent components, this means that the coherent component is necessarily lower than the total transmitted intensity.

The final feature which we would to have explain is the observation that the measured transmitted intensity is relatively stable over time while the measured heterodyne signal fluctuates greatly widely over the time scale of 0.1 - 1 s when the coherent scattered component is a significant portion of the measured intensity. As mentioned earlier, this fluctuation is large enough that the computed coherent intensity at one time can be up to 3 times higher than at another.

4.2 Two Simple Models

We shall presently consider a simplified description of our experiment. This description will include the important and relevant aspects of the experiment while unimportant features will be suppressed for now. Having completed this description, we will then present two very simple models to better understand the issues involved in explaining the three features mentioned above.

The biggest simplification involved in this analysis is the assertion that the ballistic component of the transmitted light has a wavefront which is parallel to the surface of the detector. With this assertion, the phase of the ballistic light component will be constant over the detector area. Its electric field shall be expressed as $E_B e^{i(\omega + \Delta\omega)t}$. This is obviously not the case in the experiment; the direction of the transmitted ballistic component is not at right angles to the detector area. Therefore, in reality, the phase is position dependent. We shall examine the impact of this later in the analysis. We shall

also assume that the reference beam has a wavefront which is parallel to the detector. Its electric field shall be expressed as $E_r e^{i\omega t}$. This is a reasonable reflection of reality, since in the experiment the detection system is aligned in the direction of the reference beam. Finally, we allow for an arbitrary wavefront for the scattered light component. Its electric field can be expressed as $E_{scattered}(x,y)e^{i(\omega+\Delta\omega)t}e^{i\delta(x,y)}$.

The transmitted intensity measurement can be expressed as:

$$\bar{I}_{transmitted} = \frac{1}{A}\iint_{x,y}\left|(E_B + E_{scattered}(x,y)e^{i\delta(x,y)})\right|^2 dxdy \tag{4.1}$$

where the integration is done over the total area A of the detector.

The heterodyne signal can likewise be expressed as:

$$Heterodyne\ Signal = \frac{1}{A}\mathrm{Re}\left(\iint_{x,y}2E_r(E_B + E_{scattered}(x,y)e^{i\delta(x,y)})e^{i\Delta\omega t}dxdy\right) \tag{4.2}$$

where the $e^{i\Delta\omega t}$ term gives the heterodyne oscillation. We can extract the amplitude of the oscillation by reexpressing the equation as

$$I_{hetero} = \frac{1}{A}\left|\iint_{x,y}2E_r(E_B + E_{scattered}(x,y)e^{i\delta(x,y)})dxdy\right| \tag{4.3}$$

If we determine $a(A,\theta(x,y,t),\Delta\omega)$ by calibration with respect to the initial ballistic transmitted intensity, it can be seen that $a(A,\theta(x,y,t),\Delta\omega)$ in this case will be 2. The predicted coherent intensity is then given by (2.8) with the appropriate $a(A,\theta(x,y,t),\Delta\omega)$:

$$I_{s,coh} = \frac{I_{hetero}^2}{4I_r}$$

(4.4)

4.2.1 Conventional Model

The assumption in conventional theories that scattered light preserves no coherence translates in this model to a rapidly and randomly varying $\delta(x,y)$ where the time scale of the variation is much shorter than the time period of 1 heterodyne oscillation. This has the effect that if we time average the preceding equations on a time scale comparable to this variation rate, any terms which shows a cosine dependence on $\delta(x,y)$ drops out.

If we assume for simplicity that $E_{scattered}(x,y)$ is constant over the whole area of the detector, the measured intensity will be given by:

$$\begin{aligned}\overline{I}_{transmitted} &= E_B^2 + E_{scattered}^2 \\ &= I_B + I_{scattered}\end{aligned}$$

(4.5)

The heterodyne amplitude will be given by:

$$I_{hetero} = 2E_r E_B$$

(4.6)

and the corresponding computed coherent intensity is:

$$I_{s,coh} = E_B^2 = I_B$$

(4.7)

The important consequence of this computation is that this simple conventional model predicts that the transmitted intensity can be expressed as the sum of the ballistic

component and the scattered component. In addition, the observed coherent component will always be equal to the ballistic component.

This model is therefore flawed because it cannot account for our observation that the coherent intensity is experimentally measured to be larger than the ballistic component. In other words, this model predicts a coherent curve that parallels the exponential attenuation of the ballistic component with increasing average number of scattering events; the experiment clearly showed a significant departure from this.

4.2.2 Coherent Plane Wavefront Model

In another simple model, we can assume that scattered light is coherent and presents a uniform wavefront that is parallel to the detector area. As in the above model, we shall also assume that $E_{scattered}(x, y)$ is constant over the whole area of the detector. The assumption of parallel and uniform wavefront at the detector implies that $\delta(x, y)$ is a constant at all points on the detector.

Putting all these into the transmitted intensity equation, we get

$$
\begin{aligned}
\bar{I}_{transmitted} &= \left| (E_B + E_{scattered} e^{i\delta}) \right|^2 \\
&= E_B^2 + E_{scattered}^2 + 2E_B E_{scattered} \cos(\delta)
\end{aligned}
\tag{4.8}
$$

Not surprisingly, the transmitted intensity now depends on the phase angle δ. This dependency also shows up in the heterodyne amplitude:

$$
\begin{aligned}
I_{hetero} &= \left| 2E_r (E_B + E_{scattered} e^{i\delta}) \right| \\
&= 2E_r \sqrt{E_B^2 + E_{scattered}^2 + 2E_B E_{scattered} \cos(\delta)}
\end{aligned}
\tag{4.9}
$$

The computed coherent intensity is

$$I_{s,coh} = E_B{}^2 + E_{scattered}{}^2 + 2E_B E_{scattered}\cos(\delta)$$ (4.10)

It can be seen that the computed intensity $I_{s,coh}$ is equal to $\bar{I}_{transmitted}$. This simple model would therefore predict that the coherent intensity profile will be superposed on the top of the transmitted intensity curve. This conclusion is in disagreement with the experimental observed feature that the coherent intensity profile is lower than the transmitted intensity curve.

It is interesting to note that we have seen two different models which computed the coherent intensity profile to be either given by the ballistic component profile or the transmitted intensity profile. In the light of the analysis of these models, we shall next present an improvement for the theory that would predict a coherent intensity profile which is in between the two limits and offer a mechanism to account for the slow fluctuation in the heterodyne signal amplitude.

4.3 Improved Theory

It is necessary for us to take a closer look at the behavior of $E_{scattered}(x,y)$ and $\delta(x,y)$ so that we can better model their behavior. As such, we shall first analyze how the two terms arise from the formulation of multiple paths approach to the scattering problem.

The electric field at any point on the detector area can be written as the electric field contribution from all possible individual paths through the turbid medium. The exact expression for each of these possible paths can be written as

$$E_q e^{i\theta_q} e^{i\omega t} = E_{input} e^{i\omega t} e^{ikL_q} \prod_{m=1}^{n_q} r_m \qquad (4.11)$$

where L_q is the path difference between the qth trajectory and the ballistic photons trajectory. kL_q is the phase delay relative to the straight path to the detector as introduced by this additional path length L_q producted with the wavevector k in the turbid medium. r_m is the proportion of incident light scattered along the specified path at the mth microsphere and n_q is the total number of microspheres involved in this particular path. It is important to note that paths followed by ballistic photons are not to be counted in this summation of trajectories, as the electric field for ballistic component is already accounted for by the electric field E_B.
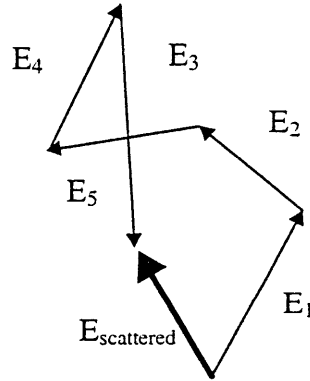

Figure 4.2: The vectorial sum of electric field from all possible paths gives the observed electric field.

In this formulation, we are assuming that scattering from each individual microspheres is entirely coherent. This is in contradiction to the assumption made in conventional theories, but it seemed a reasonable one to assert that no random phase jitter

should be ascribed to this simple physical problem of scattering. By asserting thus, we must look for mechanism elsewhere in the problem that will at least give an appearance of loss of coherence, so that we can reconciliate with the experimental findings that the computed coherent intensity is less than the transmitted intensity.

$E_{scattered}(x,y)$ and $\delta(x,y)$ can be expressed as a summation of all possible paths as such:

$$E_{scattered}(x,y)e^{i\delta(x,y)}e^{i\omega t} = \sum_q E_q e^{i\theta_q} e^{i\omega t} \qquad (4.12)$$

We can interpret this as a vectorial sum of many small contribution terms with magnitude given by E_q and angle of inclination θ_q as shown in Fig. 4.2.

Given enough paths, it can be seen that the amplitude of the resulting electric field can be well approximated by the square root of the sum of the squares of the electric field of each path. Specifically,

$$
\begin{aligned}
E_{scattered}(x,y) &= \sqrt{\sum_{q1}\sum_{q2} E_{q1}E_{q2}e^{i(\theta_{q1}-\theta_{q2})}} \\
&= \sqrt{\sum_q E_q^2 + \sum_{q1 \neq q2} E_{q1}E_{q2}e^{i(\theta_{q1}-\theta_{q2})}} \qquad (4.13) \\
&\approx \sqrt{\sum_q E_q^2}
\end{aligned}
$$

where $\sum_{q1 \neq q2} E_{q1}E_{q2}e^{i(\theta_{q1}-\theta_{q2})}$ is much smaller than $\sum_q E_q^2$ due to the phase averaging.

As long as the number of possible independent paths is large, we can effectively ignore the phase factors of the individual paths when calculating the amplitude . In the typical experiment, the total number of microspheres that is within the region illuminated

74

by the input signal beam is on the order of 100,000. This implies that even if we only consider paths involving single scattering events only, the number of independent paths will be on the order of 100,000. The dropping of cross terms in (4.13) is therefore valid.

In addition, it is reasonable to assert that $E_{scattered}(x, y)$ is constant over the small area of the detector. E_q from each scattering path is not expected to be significantly altered by small angular angles changes as long as the angular changes are much smaller than the typical phase function angle which in the case of the microspheres is about 0.42 rad. Our detector area subtends an angle of about 2 mrad from the turbid medium, as such it is reasonable to expect E_q for each path to remain constant over the area of the detector. Since $E_{scattered}(x, y)$ is given by $\sum_{q} E_q^2$, we can therefore also expect $E_{scattered}(x, y)$ to be constant over the detector area.

$\delta(x, y)$, however, cannot be simplified thus. Slight displacement of the point of consideration on the detector area can lead to changes in the phase angle of each contributing vector. The sum of these contributions can significantly alter $\delta(x, y)$. In addition, $\delta(x, y)$ can vary in time, because the Brownian motion of the microspheres in the solution will continuously alter the optical path length of each individual paths.

In the light of this better understanding, we can rewrite equation (4.1) - (4.4) as:

$$\bar{I}_{transmitted} = \frac{1}{A} \iint_{x,y} \left| (E_B + E_{scattered} e^{i\delta(x,y)}) \right|^2 dxdy \tag{4.14}$$

$$I_{hetero} = \frac{1}{A} \left| \iint_{x,y} 2E_r (E_B + E_{scattered} e^{i\delta(x,y)}) dxdy \right| \tag{4.15}$$

75

$$I_{s,coh} = \frac{1}{A^2} \left| \iint_{x,y} (E_B + E_{scattered} e^{i\delta(x,y)}) dx dy \right|^2 \tag{4.16}$$

(4.14) leads to an evaluated form given by:

$$\begin{aligned}
\bar{I}_{transmitted} &= E_B{}^2 + E_{scattered}{}^2 + 2E_B E_{scattered} \iint_{x,y} \cos(\delta(x,y)) dx dy \\
&= I_B + I_{scattered} + 2\sqrt{I_B I_{scattered}} \iint_{x,y} \cos(\delta(x,y)) dx dy
\end{aligned} \tag{4.17}$$

If $\delta(x,y)$ is non-uniform over the detector area, as argued, the last term can be very small in relation to the first two after the integration. In addition, the last term is the only one where $\delta(x,y)$ can vary as changes over time due to slow drifts of the microspheres.

In the experiment, we did not observe any fluctuation in the measurement of the transmitted intensity above the laser fluctuation. Therefore, the last term of (4.17) must be reasonably small, which indicates that $\delta(x,y)$ is significantly non-uniform over the detector area. If we ignore that term, (4.17) would reveal that the transmitted intensity is given approximately by the sum of the ballistic component and the scattered component; a result which earlier in this chapter has been pointed out as unobvious.

The computation of the coherent intensity cannot be as readily evaluated due to the integration. A simple approach to simplify the problem can be taken by assuming at each point on the detector, $\delta(x,y)$ is either in 0 or π. The proportion of area where they are in phase shall be called p and, consequently, the proportion of area where they are out of phase is $1 - p$. This simplifies the form of (4.16) to be as follows:

$$I_{s,coh} = \frac{1}{A^2}\left|\iint_{x,y}(E_B + E_{scattered}e^{i\delta(x,y)})dxdy\right|^2$$

$$\approx \left|p(E_B + E_{scattered}) + (1-p)(E_B - E_{scattered})\right|^2 \qquad (4.18)$$

$$\approx \left|E_B + (-1+2p)E_{scattered}\right|^2$$

$$\approx E_B^2 + (1-2p)^2 E_{scattered}^2 - 2(1-2p)E_B E_{scattered}$$

As a short time passes, we would expect the phase of the scattered component to drift a little so that areas previously where the two fields were in phase will be out of phase and where the two fields were out of phase will be in phase. This leads to the corresponding coherent intensity measurement:

$$I_{s,coh} = \frac{1}{A^2}\left|\iint_{x,y}(E_B + E_{scattered}e^{i\delta(x,y)})dxdy\right|^2$$

$$\approx \left|p(E_B - E_{scattered}) + (1-p)(E_B + E_{scattered})\right|^2 \qquad (4.19)$$

$$\approx \left|E_B + (1-2p)E_{scattered}\right|^2$$

$$\approx E_B^2 + (1-2p)^2 E_{scattered}^2 + 2(1-2p)E_B E_{scattered}$$

If we further assume that the interchange between (4.18) and (4.19) occur repeatedly over a time scale shorter than the lock-in amplifier's integration time scale of 100ms, then the actual measured coherent intensity is given by the average of the two equations:

$$I_{s,coh,ave} \approx E_B^2 + (1-2p)^2 E_{scattered}^2$$

$$\approx I_B + (1-2p)^2 I_{scattered} \qquad (4.20)$$

From this equation, if the proportion are exactly balanced so that $p = \frac{1}{2}$, then we will see a coherent intensity profile that is the same as the ballistic component profile. If there is a slight mismatch, then the coherent intensity profile will necessarily be higher

than the ballistic component's profile but lower than the transmitted intensity profile as given by (4.17).

This model can therefore effectively explain the first two features mentioned in the beginning of the chapter. The coherent intensity profile is necessarily bounded between the ballistic component profile and the transmitted intensity profile. As long as there is a slight mismatch in the distribution of $\delta(x, y)$, the coherent intensity profile will be located somewhere between the two.

This model will also be able to account for the third feature mentioned. In addition to the effect of averaging (4.18) and (4.19) over short time scale by small relative displacements of the microspheres, there can also be substantial drifts over larger distances over a longer time scale of 0.1 - 1 s. These more substantial drifts can dramatically alter the individual contribution optical paths. The net result would be an alteration of the proportion factor p. This long time scale fluctuation of p will then lead to the observation that the heterodyne signal amplitude fluctuates slowly over time.

In summary, we believe this model can adequately explain the experimental results. The experimental observation that the coherent intensity is larger than the ballistic component is due to the fact that scattered light has coherence. The observation that the coherent intensity is smaller than the total transmitted intensity can be attributed to the non-uniform scattered light wavefront which leads to some averaging out the heterodyne signal over the area of the detector. Finally, the observed fluctuation in the coherent intensity measurement can be attributed to slow drifts of the microspheres which alters the non-uniform wavefront over long time scale leading to a fluctuation in heterodyne signal amplitude.

Chapter 5

Future Directions

The model described in Chapter 4 can explain the main experimental observations; it asserts that coherence is preserved in scattered photons, and that the limited coherence that can be experimentally observed is due to the fact that the coherent scattered light has a non-uniform wavefront.

It is, however, difficult to quantitatively apply this model to fit the experimental data we have so far. The reason is the experiments were done with a signal beam that is tilted with respect to the detector area. This creates a ballistic component wavefront which is not parallel to the detector area. As such, this gives a position dependence to the phase attached to the electric field E_B. On the other hand, the theoretical model is based on a ballistic component wavefront that is parallel to the detector area. While it does not affect the qualitative features of the experiment, this complication makes it difficult to quantify the model to fit the experimental data.

In the next series of experiments that we plan to do, we should try to arrange the experiment to conform better to the model. In other words, we would like to arrange the experiment so that the ballistic component presents an approximately parallel wavefront to the detector area. It appears that this can be done by displacing the signal beam laterally rather than tilting the direction of the signal beam.
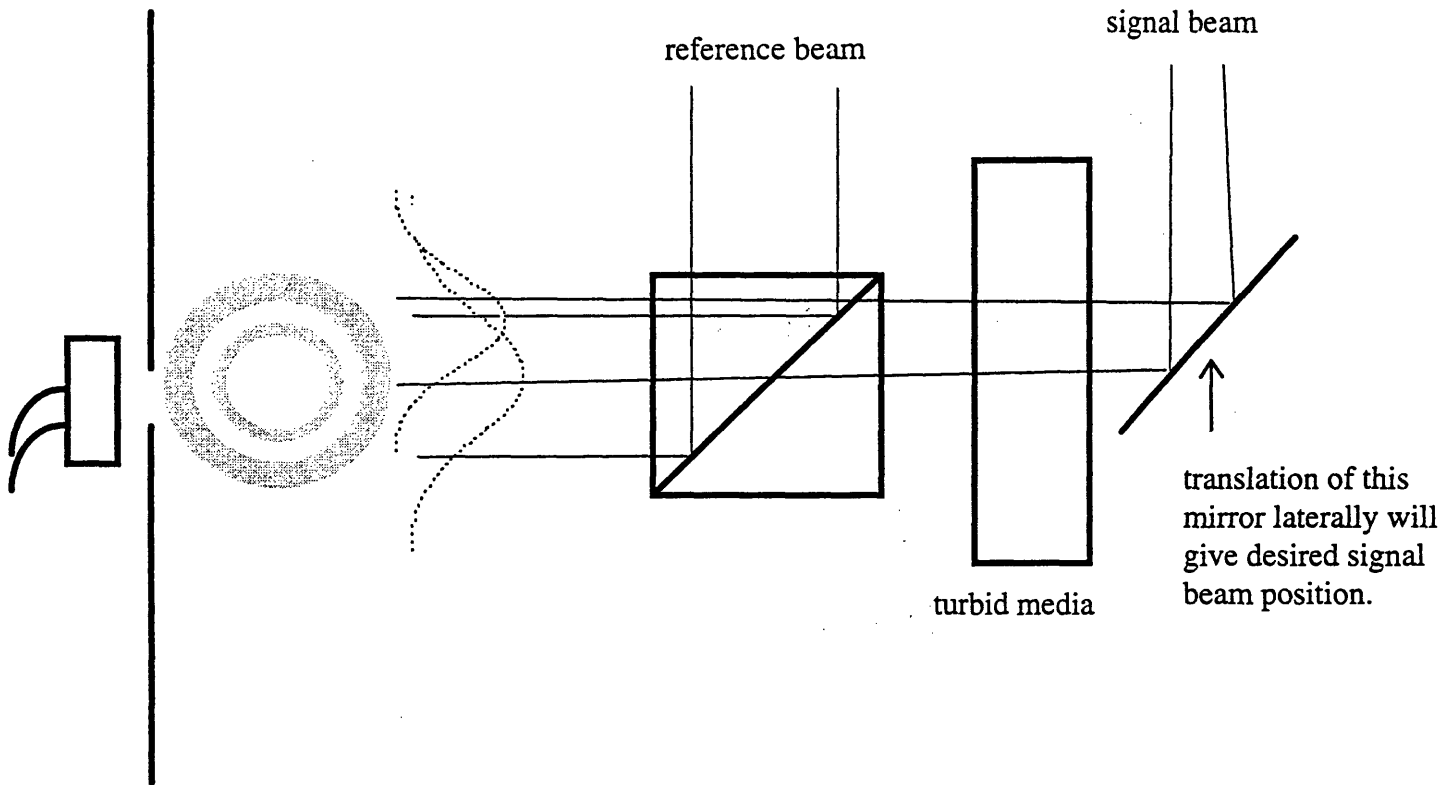
Figure 5.1: We plan to translate the signal beam laterally in the next set of experiment. This will reduce the ballistic light intensity incident on the detector area while preserving a parallel wavefront on the detector.

By doing such, we will still be able to shift the center of the signal beam away from the detector area and so lessen the amount of ballistic light incident on the detector. This will allow for detection of small amounts of scattered light as demonstrated in the second set of experiments described in Chapter 2. The advantage in doing this is that the signal beam's direction will not be altered and thus it will have a more or less parallel wavefront at the detector area.

In addition, we would also like to focus and collimate both the signal and reference beams so that they have smaller beam width. In so doing, we can shrink the size

of the detection area as well. This should help us to get a better measurement of the coherent intensity as a smaller detection area, and it will imply that less non-uniformity of the scattered light wavefront will be incident on the detection area. This leads to less averaging off of the heterodyne signal and therefore we should get a better measurement of the coherent intensity profile.

Eventually, we hope to be able to reduce the detector size enough so that the scattered wavefront as seen by the detector is approximately uniform. This will lead to an asymptotically maximal heterodyne signal. By such means, we will then be able to quantify the size of non-uniformity in the wavefront.

Chapter 6

Conclusion

The foregoing chapters detailed our successful construction of heterodyne based coherence detection system and its application to detect and measure the extent of coherence in scattered light. We would like to summarize some of the facts we learnt about the coherent scattered light here and the reasonable explanation that can be made from our model of scattering.

We found that scattering from the microspheres observed in the experiments can be modeled as a coherent process. This is consistent with the conventional wisdom that scattering from refractive index interfaces is a coherent process; in comparison, the conventional turbid medium based scattering theories assume that scattering does not preserve coherence is an excellent assumption for intensity based computation, which greatly simplifies such computation. However, in certain situations, such as the one that pertains to our experiment, the latter can lead to disagreement with experimental observations.

The observation that the coherent intensity computed from heterodyne measurement is less than the total transmitted intensity can be explained by modeling the scattered component's wavefront as non-uniform. This leads to some averaging away of the heterodyne signal, leading to a lower observed coherent intensity.

With this model, we can also explain the fact that the coherent intensity is always higher than the ballistic component. The ballistic component is invariant of the phase drifts as introduced by movements of the microspheres; in the worst case, where the wavefront of the scattered light is extremely non-uniform over the area of the detector due to the arrangement of the microspheres, a baseline heterodyne signal corresponding to the ballistic component will still be obtained when averaged over a reasonable time scale.

In addition, the model can account for the observation that the heterodyne signal, and consequently the computed coherent intensity, fluctuates slowly over time. As the microspheres drifts, the wavefront from the scattered light changes gradually. When it is more uniform than usual, a large heterodyne signal is obtained as less averaging away of the signal takes place over the detector area. The reverse holds as well when the wavefront is more non uniform.

In future experiments, this model can be tested by arranging the experiment to be more similar to the model. At the same time, the implication from the model that there is non-uniformity in the wavefront can be tested out as well by gradually decreasing the detection area. An asymptotically maximal heterodyne signal will be obtained when the detection area becomes comparable in size to the non-uniformity.

Bibliography

1.   K. M. Yoo and R. R. Alfano, "Time-resolved coherent and incoherent components of forward light scattering in random media", *Optics Letters*, Vol. 15, No. 6 (1990).

2.   L. T. Perelman, J. Wu, I. Itzhan and M. S. Feld, "Photon migration in turbid media using path integrals", *Physics Review Letters*, 72, 1341-1344 (1994).

3.   A. Ishimaru, *Wave Propagation and Scattering in Random Medium Vol. 2*, Academic, New York, 1978.

4.   M. Toida, M. Kondo, T. Ichimura and H. Inaba, "Two-Dimensional Coherent Detection Imaging in Multiple Scattering Media Based on the Directional Resolution Capability of the Optical Heterodyne Method", *Applied Physics B* 52, 391-394 (1991).

5.   J. A. Izatt, M. R. Hee, G. M. Owen, E. A. Swanson and J. G. Fujimoto, "Optical Coherence Microscopy in Scattering Media", *Optics Letters*, Vol. 19, No. 8 (1994).

6.   B. Bouma, G. J. Tearney, S. A. Boppart, M. R. Hee, M. E. Brezinski and J. G. Fujimoto, "High-resolution Optical Coherence Tomographic Imaging using a Mode-Locked Ti:Al_2O_3 laser source", *Optics Letters*, Vol. 20, No. 13 (1995).

7.   M. R. Hee, J. A. Izatt, J. M. Jacobson, J. G. Fujimoto and Eric Swanson, "Femtoseond Transillumination Optical Coherence Tomography", *Optics Letters*, Vol. 18, No. 12 (1993).

8.   W. A. de Rooij and C. C. A. H. van der Stap, "Expansion of Mie scattering matrices in generalized spherical functions", *Astron. Astrophysics.* 131, 237-248 (1984).

9.   T. Sawatari, *Applied Optics*, Vol. 12, No. 11 (1973).

10.   W. Memdendall, et al., *Mathematical Statistics with Applications* (Third Edition). Duxbury Press, 1986.

11.   E. P. Ippen, *Nonlinear Optics*, class notes for 6.634.